

Cite this: *J. Mater. Chem. C*,  
2024, 12, 10562Received 6th May 2024,  
Accepted 8th June 2024

DOI: 10.1039/d4tc01846j

rsc.li/materials-c

# Optical properties of Ga<sub>2</sub>O<sub>3</sub> thin films grown by atomic layer deposition using GaI<sub>3</sub> and O<sub>3</sub> as precursors

Lauri Aarik, \* Hugo Mändar, Aarne Kasikov, Aivar Tarre and Jaan Aarik

Properties of Ga<sub>2</sub>O<sub>3</sub> thin films grown by atomic layer deposition from GaI<sub>3</sub> and O<sub>3</sub> on Si(100) and amorphous SiO<sub>2</sub> substrates were investigated. The Ga<sub>2</sub>O<sub>3</sub> films deposited on the bare Si and SiO<sub>2</sub> substrates at 450–550 °C contained the κ-Ga<sub>2</sub>O<sub>3</sub> phase while it was not possible to exclude the presence of the ε-Ga<sub>2</sub>O<sub>3</sub> phase in these films, either. On the substrates coated with α-Cr<sub>2</sub>O<sub>3</sub>, α-Ga<sub>2</sub>O<sub>3</sub> was obtained at 275–550 °C. The formation of crystalline phases caused a marked increase in the density, roughness, and in the growth rate as well. The refractive indices, determined for the κ/ε-Ga<sub>2</sub>O<sub>3</sub> and α-Ga<sub>2</sub>O<sub>3</sub> films with thicknesses over 70 nm, were 1.96 ± 0.03 and 2.01 ± 0.02, respectively. Corresponding values of amorphous films, deposited on Si at 150–425 °C, on SiO<sub>2</sub> at 310 °C, and on α-Cr<sub>2</sub>O<sub>3</sub>/Si at 200–234 °C, were 1.86 ± 0.03 at 633 nm. The optical bandgap energies of amorphous Ga<sub>2</sub>O<sub>3</sub>, κ/ε-Ga<sub>2</sub>O<sub>3</sub>, and α-Ga<sub>2</sub>O<sub>3</sub> were found to be 4.96, 5.22–5.28, and 5.28 eV in the approximation of direct optical transitions and 4.27, 4.43, and 5.09 eV, respectively, in the approximation of indirect optical transitions. The films of κ/ε-Ga<sub>2</sub>O<sub>3</sub> and α-Ga<sub>2</sub>O<sub>3</sub> served as effective antireflection coatings on the surface of silicon reducing the reflection down to 0.20% and 0.12%, respectively.

## 1. Introduction

Gallium oxide (Ga<sub>2</sub>O<sub>3</sub>) has attracted marked interest as a promising material for high-voltage electronic devices,<sup>1–3</sup> high electron-mobility transistors,<sup>4</sup> resistive switching memories,<sup>5,6</sup> solar-blind radiation detectors,<sup>7–9</sup> and scintillators.<sup>10</sup> Gallium oxide has also been studied as a relatively hard material<sup>11,12</sup> that can, therefore, be used in protective coatings. Furthermore, possibilities for application of Ga<sub>2</sub>O<sub>3</sub> for surface passivation of silicon solar cells have been recently investigated.<sup>13</sup> Owing to appropriate refractive index values and the relatively wide transparency gap of Ga<sub>2</sub>O<sub>3</sub> extending from the infrared to the ultraviolet spectral range,<sup>13–18</sup> Ga<sub>2</sub>O<sub>3</sub> thin films can also be used in antireflective coatings of solar cells and photodetectors that are based on silicon and III–V materials. Additionally, Ga<sub>2</sub>O<sub>3</sub> films could be applied as antireflective coatings of light-emitting diodes and diode lasers as well. In all these applications, high hardness is highly beneficial to ensure improved durability of the functional coatings.

As shown previously, the optical properties of Ga<sub>2</sub>O<sub>3</sub> thin films significantly depend on the crystal structure and phase composition formed in the deposition or post-deposition annealing process. Ga<sub>2</sub>O<sub>3</sub> can be amorphous or form at least

six crystalline phases: α-, β-, γ-, δ-, ε-, and κ-Ga<sub>2</sub>O<sub>3</sub>.<sup>19,20</sup> A marked number of studies including the characterization of refractive index (*n*) and optical bandgap (*E<sub>g</sub>*) have been conducted for amorphous films.<sup>13–18,20–26</sup> The results obtained indicate that the optical properties of the amorphous films markedly depend on the deposition method<sup>13</sup> as well as deposition process parameters.<sup>21</sup> For instance, the bandgap values of 4.05–5.47 eV<sup>13–15,17,18,20,21,23–26</sup> have been reported for amorphous Ga<sub>2</sub>O<sub>3</sub> films from the (*αhν*)<sup>2</sup> versus *hν* plots, where *α* is the absorption coefficient and *hν* is the photon energy. The refractive index values reported for amorphous films range from 1.75 to 1.90 at 633 nm.<sup>13–18,21,22,24,25</sup>

In the list of crystalline phases, β-Ga<sub>2</sub>O<sub>3</sub> with the monoclinic structure (space group *C2/m*) has attracted the most significant interest that is evidently related to the higher stability of this phase compared to the stabilities of other crystalline phases.<sup>19,20</sup> Optical bandgap energies of 4.26–5.24 eV published for β-Ga<sub>2</sub>O<sub>3</sub><sup>14,16,24–31</sup> are comparable to those of amorphous films while *n* values of 1.83–1.94 at 633 nm have been reported for β-Ga<sub>2</sub>O<sub>3</sub>.<sup>14,16,22,25,27,28,30</sup>

A marked number of publications have also been focused on optical properties of α-Ga<sub>2</sub>O<sub>3</sub> (space group *R3c*) because this phase has high density and *E<sub>g</sub>* values.<sup>19,20</sup> For instance, the *E<sub>g</sub>* values ranging from 5.04 to 5.36 eV have been determined from the (*αhν*)<sup>2</sup> versus *hν* curves recorded for α-Ga<sub>2</sub>O<sub>3</sub> thin films in the vicinity of the absorption edge.<sup>20,26,32–35</sup> A similar value

Institute of Physics, University of Tartu, W. Ostwaldi 1, 50411 Tartu, Estonia.  
E-mail: lauri.aarik@ut.ee

(5.46 eV) for the lowest band-to-band transition energy was obtained for  $\alpha$ -Ga<sub>2</sub>O<sub>3</sub> from the analysis based on spectroscopic ellipsometry (SE) measurements and density functional theory calculations.<sup>36</sup> The spectroscopic studies have also demonstrated that the absorption spectra of  $\alpha$ -Ga<sub>2</sub>O<sub>3</sub> have a more complex shape<sup>36–39</sup> that has been interpreted assuming contribution of an exciton and two band-to-band transitions with bandgap energies of 5.58–5.62 and 6.18–6.44 eV, respectively.<sup>37–39</sup>

The  $\alpha$ -Ga<sub>2</sub>O<sub>3</sub> polymorph has also relatively high  $n$  values of 1.97–2.01 as can be determined from the real parts of dielectric constants determined from SE data.<sup>36,39</sup> However, the information concerning this parameter and, particularly, its dependence on the deposition process parameters is still limited.

Hexagonal  $\epsilon$ -Ga<sub>2</sub>O<sub>3</sub> (space group  $P63mc$ ) and orthorhombic  $\kappa$ -Ga<sub>2</sub>O<sub>3</sub> (space group  $Pna2_1$ ) are also known as polymorphs with relatively high density.<sup>19,40,41</sup> According to theoretical calculations, the bandgap energies of  $\epsilon$ -Ga<sub>2</sub>O<sub>3</sub> and  $\kappa$ -Ga<sub>2</sub>O<sub>3</sub> should be 4.27 and 4.62 eV, respectively.<sup>42</sup> However, the experimental characterization of optical parameters of pure  $\epsilon$ - and  $\kappa$ -Ga<sub>2</sub>O<sub>3</sub> polymorphs is a complex task because it is difficult to reveal the presence or absence of  $\epsilon$ -Ga<sub>2</sub>O<sub>3</sub> in the thin films that contain  $\kappa$ -Ga<sub>2</sub>O<sub>3</sub>.<sup>40,41</sup> Moreover, the unambiguous determination of the  $\kappa$ -Ga<sub>2</sub>O<sub>3</sub> phase in thin films by the X-ray diffraction (XRD) method needs rather complex measurements.<sup>43,44</sup> This is probably one reason for the limited number of papers reporting the  $E_g$  values of  $\epsilon$ -Ga<sub>2</sub>O<sub>3</sub> and  $\kappa$ -Ga<sub>2</sub>O<sub>3</sub>. In these publications,  $E_g$  values of 4.6–5 eV for  $\epsilon$ -Ga<sub>2</sub>O<sub>3</sub><sup>45,46</sup> and 4.9–5.14 eV for  $\kappa$ -Ga<sub>2</sub>O<sub>3</sub><sup>9,29,47,48</sup> have been reported. Notably, even less information can be found for  $n$  of these polymorphs while the value of 1.6 reported for  $\epsilon$ -Ga<sub>2</sub>O<sub>3</sub> does not seem to be consistent with the relatively high density of this phase.<sup>19</sup> Therefore, additional studies focused on the optical properties of  $\epsilon$ -Ga<sub>2</sub>O<sub>3</sub> and  $\kappa$ -Ga<sub>2</sub>O<sub>3</sub> as well as  $\alpha$ -Ga<sub>2</sub>O<sub>3</sub> polymorphs are evidently needed.

The self-limiting nature of atomic layer deposition (ALD) enables synthesis of thin films controlling the thickness with sub-nanometre resolution,<sup>15–18,24,44</sup> fabrication of conformal coatings on substrates with complex shapes,<sup>14,15,22</sup> and deposition of films with uniform thicknesses on large-area substrates.<sup>18</sup> However, the deposition of crystalline Ga<sub>2</sub>O<sub>3</sub> films on substrates that do not support epitaxial growth has been a problem for the majority of ALD processes studied so far. In a recent study, thin films containing  $\alpha$ -Ga<sub>2</sub>O<sub>3</sub> as well as those containing  $\kappa$ -Ga<sub>2</sub>O<sub>3</sub> were grown by ALD at sufficiently low growth temperatures ( $T_G$ ) using GaI<sub>3</sub> and O<sub>3</sub> as the precursors.<sup>44</sup> Therefore, this precursor system opens new possibilities for deposition and investigation of crystalline Ga<sub>2</sub>O<sub>3</sub> thin films. Moreover, the GaI<sub>3</sub>–O<sub>3</sub> precursor combination ensured relatively high growth rates as well as very low concentrations of residual impurities in the films, deposited in a wide range of  $T_G$ . For these reasons, the corresponding ALD process seems to be attractive for several applications, including technology of electronic devices, radiation detectors, waveguides, and optical coatings.

In electronics applications, the bandgap energy of a semiconductor dielectric material is a very important parameter, while in optical applications, bandgap energies as well as refractive indices and absorption coefficient values should be

known. All these parameters depend on the phase composition of a material. However, impurities, structural defects, and surface roughness that are all related to the material synthesis method may also influence the performance of materials and thin films in various applications. Hence, proceeding from the earlier promising results,<sup>44</sup> the application potential of the GaI<sub>3</sub>–O<sub>3</sub> ALD process for the deposition of Ga<sub>2</sub>O<sub>3</sub> thin films for optical applications was studied in the present work. For this purpose, films containing different Ga<sub>2</sub>O<sub>3</sub> phases were deposited. The effect of substrates and ALD process parameters on the properties of the films was investigated. Significant effects of crystallization processes on the optical properties as well as growth rate were revealed. Application of Ga<sub>2</sub>O<sub>3</sub> as a material of antireflection (AR) coatings was studied.

## 2. Experimental details

The Ga<sub>2</sub>O<sub>3</sub> thin films were deposited on Si(100), amorphous SiO<sub>2</sub>,  $\alpha$ -Cr<sub>2</sub>O<sub>3</sub>/Si(100), and  $\alpha$ -Cr<sub>2</sub>O<sub>3</sub>/SiO<sub>2</sub> substrates in a low-pressure flow-type ALD reactor described earlier.<sup>49</sup> The  $\alpha$ -Cr<sub>2</sub>O<sub>3</sub> seed layers that were needed to grow  $\alpha$ -Ga<sub>2</sub>O<sub>3</sub> films were also deposited by ALD. The seed layer thicknesses ( $d_{SL}$ ) ranged from 0.7 to 9 nm. The ALD and post growth annealing processes employed to obtain  $\alpha$ -Cr<sub>2</sub>O<sub>3</sub> are described in a previous paper.<sup>50</sup>

During ALD of Ga<sub>2</sub>O<sub>3</sub>, GaI<sub>3</sub> (99%, Strem Chemicals, Inc.) used as a metal precursor was kept at a temperature of 130 °C to volatilize the precursor. The GaI<sub>3</sub> vapour was transferred to the reaction zone with N<sub>2</sub> (AS Linde Gas, 99.999%) that was used as a carrier and purge gas. O<sub>3</sub> employed as an oxygen precursor was generated in a BMT Messtechnik 802N generator from O<sub>2</sub> (AS Linde Gas, 99.999%). The O<sub>3</sub> concentration, measured using a BMT Messtechnik 964 analyser at the output of the ozone generator, was set at 220–250 g m<sup>−3</sup>. An ALD cycle, repeated to obtain films with expected thicknesses ( $d$ ), contained a GaI<sub>3</sub> pulse, purge, O<sub>3</sub> pulse, and another purge. Each of these reaction steps was 2 s in duration. For the deposition of Ga<sub>2</sub>O<sub>3</sub> films studied in the present work, 500–2000 ALD cycles were used.

The elemental composition of the films was characterized using an X-ray fluorescence (XRF) spectrometer ZSX-400 (Rigaku Corp.). The phase composition, texture, density, and surface roughness were determined using an X-ray diffractometer Smartlab (Rigaku Corp.) with CuK $\alpha$  radiation generated at a tube power of 8.1 kW. Grazing incidence X-ray diffraction (GIXRD) carried out at an incidence angle  $\omega = 0.5^\circ$ , coplanar  $\theta$ – $2\theta$ -XRD and non-coplanar XRD were applied for phase composition and texture studies, while the X-ray reflection (XRR) method was used for the thickness, density, and surface roughness characterization. Crystalline phases observed in the films were identified on the basis of powder diffraction database ICDD PDF-2 (version 2023) and/or single crystal database ICSD (version 2022).

Optical properties were investigated using a spectroscopic ellipsometer GES-5E (Semilab, Inc.) and spectrophotometer V-570 (Jasco, Inc.). The  $n$  values were determined from the SE data as well as from the spectral oscillations of optical transmission spectra.<sup>51</sup> To analyse the SE data for the Ga<sub>2</sub>O<sub>3</sub> films



deposited on Si and SiO<sub>2</sub> substrates, one-layer fitting was used. In the case of films deposited on the  $\alpha$ -Cr<sub>2</sub>O<sub>3</sub> seed layers, an additional layer was added to the model that the fitting was based on. The thickness of this layer was calculated together with that of the Ga<sub>2</sub>O<sub>3</sub> film. The absorption spectra were calculated from the transmission and reflection spectra<sup>52</sup> measured at normal incidence in a wavelength ( $\lambda$ ) range of 190–800 nm.

### 3. Results and discussion

#### 3.1. Phase composition

Consistent with the results of earlier studies,<sup>44</sup> the X-ray diffractograms depicted in Fig. 1(a) and (b) demonstrate that

the films deposited on Si at  $T_G \geq 425^\circ\text{C}$  and on  $\alpha$ -Cr<sub>2</sub>O<sub>3</sub>/Si at  $T_G \geq 275^\circ\text{C}$  contained crystalline phases, while the films deposited at lower  $T_G$  were amorphous. The crystalline phases, identified on the basis of diffractograms presented in Fig. 1(a) and (b), were  $\epsilon$ -Ga<sub>2</sub>O<sub>3</sub> and/or  $\kappa$ -Ga<sub>2</sub>O<sub>3</sub> on bare Si substrates and  $\alpha$ -Ga<sub>2</sub>O<sub>3</sub> on  $\alpha$ -Cr<sub>2</sub>O<sub>3</sub>/Si. The same phases were obtained on bare SiO<sub>2</sub> and  $\alpha$ -Cr<sub>2</sub>O<sub>3</sub>/SiO<sub>2</sub> substrates, respectively (Fig. 1(c) and (d)). Regardless of the film thickness, which varied from 74 to 210 nm, and  $T_G$ , which varied from 450 to 550 °C, the highly developed preferential (0 0 1) orientation of  $\epsilon$ -Ga<sub>2</sub>O<sub>3</sub> and/or  $\kappa$ -Ga<sub>2</sub>O<sub>3</sub> was formed in the films deposited on Si (Fig. 1(a)) as well as on SiO<sub>2</sub> (Fig. 1(c)).

On  $\alpha$ -Cr<sub>2</sub>O<sub>3</sub>/Si and  $\alpha$ -Cr<sub>2</sub>O<sub>3</sub>/SiO<sub>2</sub> substrates, the (0 0 1) orientation of  $\alpha$ -Ga<sub>2</sub>O<sub>3</sub> was the prevalent one, especially in

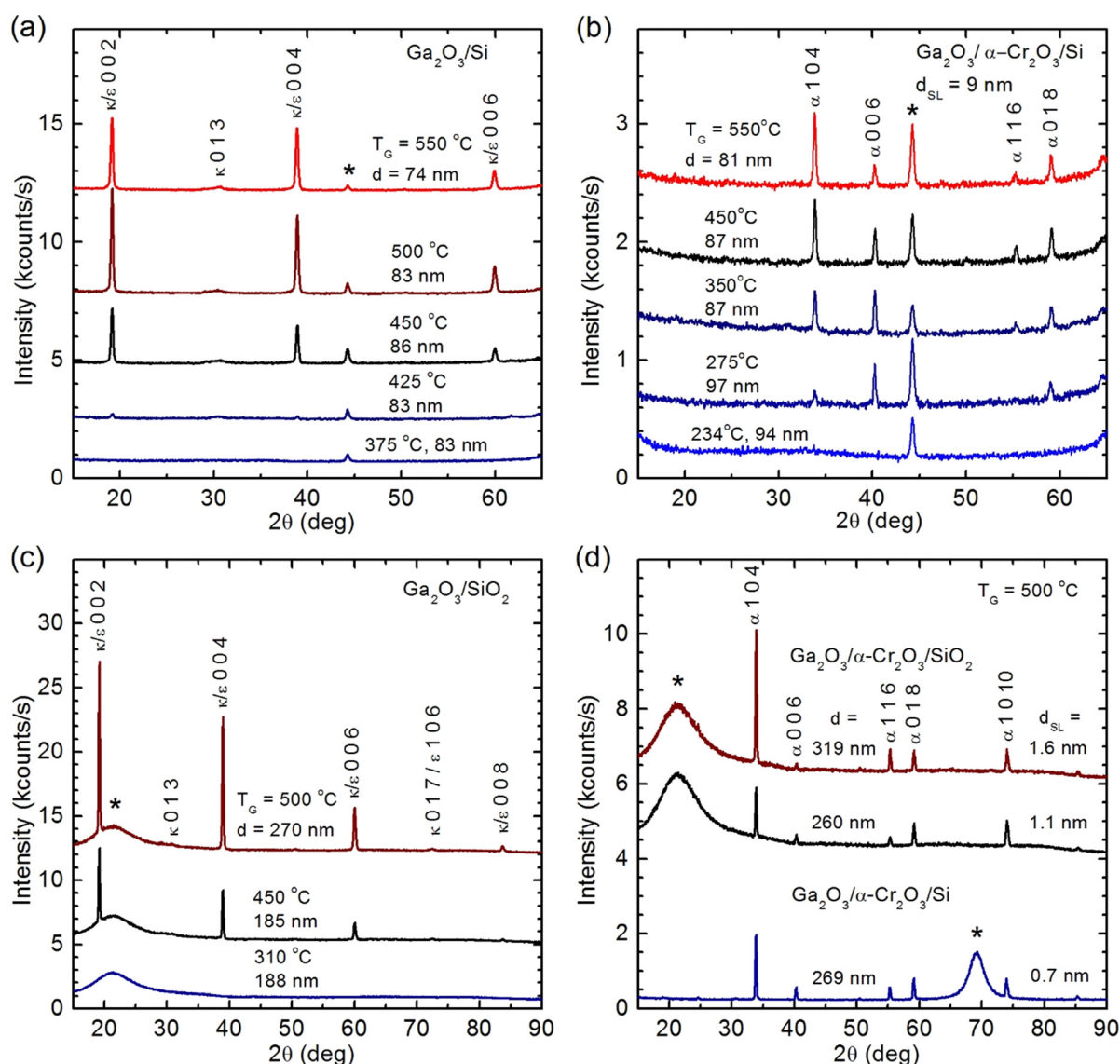


Fig. 1 Coplanar  $\theta$ - $2\theta$ -XRD diffractograms of (a), (b) 74–97 nm thick Ga<sub>2</sub>O<sub>3</sub> films grown on (a) bare Si and (b)  $\alpha$ -Cr<sub>2</sub>O<sub>3</sub>/Si substrates, and (c), (d) 185–319 nm thick Ga<sub>2</sub>O<sub>3</sub> films grown on (c) SiO<sub>2</sub> and (d)  $\alpha$ -Cr<sub>2</sub>O<sub>3</sub>/SiO<sub>2</sub> and  $\alpha$ -Cr<sub>2</sub>O<sub>3</sub>/Si substrates. Growth temperatures and film thicknesses are shown at corresponding diffractograms. (b) The  $\alpha$ -Cr<sub>2</sub>O<sub>3</sub> seed layer thicknesses ( $d_{SL}$ ) were  $9 \pm 3$  nm. Miller indices of  $\alpha$ -Ga<sub>2</sub>O<sub>3</sub> ( $\alpha$ ) and  $\kappa$ -Ga<sub>2</sub>O<sub>3</sub> ( $\kappa$ ) are added to corresponding XRD reflections. Reflections attributable to the substrates and/or sample stage of diffractometer are marked with asterisks.



the thinner films grown at lower temperatures (Fig. 1(b)). This conclusion is based on the result that the reflection 0 0 6, which has an intensity of 3% relative to the 1 0 4 reflection of an ideal polycrystalline material (PDF-2 file 01-074-1610), is the most intense one in the diffractograms of the films grown at 275–350 °C (Fig. 1(b)). However, with increasing  $T_G$  and film thickness, the relative intensity of the 0 0 6 reflection decreased (Fig. 1(b) and (d)) and approached the corresponding value of a powder material.

As the reflections of  $\epsilon$ -Ga<sub>2</sub>O<sub>3</sub> overlap with those of  $\kappa$ -Ga<sub>2</sub>O<sub>3</sub>,<sup>40,41,43,44</sup> it is not possible to conclude on the basis of the coplanar  $\theta$ -2 $\theta$  XRD diffractograms presented in Fig. 1(a) and (c), which of these two phases was formed on bare Si and SiO<sub>2</sub> substrates. However, there are a few  $\kappa$ -Ga<sub>2</sub>O<sub>3</sub> reflections, for instance reflections 0 1 3 and 1 2 2, that do not have counterparts in the diffractogram of  $\epsilon$ -Ga<sub>2</sub>O<sub>3</sub>.<sup>40,43,44</sup> Unfortunately, in the case of  $\kappa$ -Ga<sub>2</sub>O<sub>3</sub> films with highly developed (0 0 1) preferential orientation of crystallites, these reflections cannot be recorded by XRD using the coplanar  $\theta$ -2 $\theta$  geometry. Therefore, non-coplanar XRD analysis was performed to obtain more information about the phase composition of the films grown on bare Si and SiO<sub>2</sub>. In this analysis, the sample inclination angle ( $\chi$ ) was varied, while the  $\theta$ -2 $\theta$  XRD diffractograms for selected 2 $\theta$  ranges were recorded (Fig. 2).

According to the results of this analysis, the reflection observed in the coplanar diffractograms at around 30.5° (Fig. 1(a) and (c)) peaked at  $\chi = 20.5^\circ$  in the diffractogram of the film grown on Si and at  $\chi = 20.2^\circ$  in the diffractogram of the film grown on SiO<sub>2</sub> (Fig. 2). The 2 $\theta$  value of 30.7°, refined from the non-coplanar analysis, matched with the 0 1 3 reflection position of  $\kappa$ -Ga<sub>2</sub>O<sub>3</sub>. As  $\beta$ -Ga<sub>2</sub>O<sub>3</sub> could also contribute to the reflection at these 2 $\theta$  values, a  $\chi$  scan was also recorded at 48.7°

where the 5 1 0 reflection of  $\beta$ -Ga<sub>2</sub>O<sub>3</sub> with a relative intensity of 20% was expected to appear (ICSD coll. code 83645) provided that this phase was present in the films. However, the  $\chi$  scan did not reveal this reflection. Thus, there were no detectable amounts of  $\beta$ -Ga<sub>2</sub>O<sub>3</sub> in these films. Consequently, the reflection observed at 30.7° belonged to  $\kappa$ -Ga<sub>2</sub>O<sub>3</sub>. Additionally, a reflection attributable only to (1 2 2) atomic planes of  $\kappa$ -Ga<sub>2</sub>O<sub>3</sub> appeared at  $2\theta = 33.3^\circ$  and  $\chi$  values of 56.2° and 55.7° in the diffractograms of films grown on bare Si and SiO<sub>2</sub>, respectively (Fig. 2). Within a precision of 1.0–1.6°, these  $\chi$  values observed were equal to the angle between the (1 2 2) and (0 0 1) planes of  $\kappa$ -Ga<sub>2</sub>O<sub>3</sub> (54.6°). Hence, the appearance of the (1 2 2) reflection in non-coplanar and (0 0  $l$ ) reflections in coplanar analysis confirmed the presence of  $\kappa$ -Ga<sub>2</sub>O<sub>3</sub> in these films. Unfortunately, the XRD analysis did not allow us to exclude the presence of  $\epsilon$ -Ga<sub>2</sub>O<sub>3</sub> in the films deposited on bare Si and SiO<sub>2</sub>. Therefore, the phase of these films is denoted as  $\kappa/\epsilon$ -Ga<sub>2</sub>O<sub>3</sub> in the following sections of this paper.

The growth of  $\kappa/\epsilon$ -Ga<sub>2</sub>O<sub>3</sub> on substrates (such as Si and amorphous SiO<sub>2</sub>) that do not support epitaxial growth is one of the main advantages of the GaI<sub>3</sub>-O<sub>3</sub> ALD process. In previous studies, the  $\kappa$ - and  $\epsilon$ -Ga<sub>2</sub>O<sub>3</sub> have mainly been observed in the films epitaxially grown on  $\alpha$ -Al<sub>2</sub>O<sub>3</sub> (0 0 1) (c-cut sapphire) substrates,<sup>7,9,20,25,31,41,45–48</sup> whereas only in a few cases have the substrate temperatures below 500 °C been sufficient for formation of these phases.<sup>25,48</sup> Moreover, a relatively complex method, that is, epitaxial lateral overgrowth, including the deposition of the TiO<sub>2</sub> seed layer on c-sapphire and a following lithography process to form a pattern that supports the  $\kappa$ -Ga<sub>2</sub>O<sub>3</sub> growth, has been developed<sup>53</sup> and applied<sup>54</sup> for improving the quality of  $\kappa/\epsilon$ -Ga<sub>2</sub>O<sub>3</sub> films. However, even in these cases, substrate temperatures of 540–570 °C have been used for deposition of the films by halide vapour phase epitaxy.<sup>53,54</sup> Hence, the thermal ALD based on GaI<sub>3</sub> and O<sub>3</sub> provides a much simpler approach for deposition of films containing  $\kappa$ -Ga<sub>2</sub>O<sub>3</sub>.

Low concentration of impurities in the films deposited by ALD from GaI<sub>3</sub> and O<sub>3</sub> was probably a key factor that enabled growth of crystalline phases at relatively low temperatures. For instance, according to the results of XRF analysis, the iodine concentration did not exceed 0.01 at% in the 160–320-nm-thick films deposited on Si and SiO<sub>2</sub> substrates at 450–500 °C. With decreasing  $T_G$ , the iodine concentration increased reaching 0.05 at% at 310 °C and 1.5 at% at 200 °C.

### 3.2. Influence of crystallization on density, surface roughness, and growth rate

Expectedly, the densities as well as surface roughness values significantly depended on the formation of crystalline phases in the deposition process. The growth of  $\alpha$ -Ga<sub>2</sub>O<sub>3</sub> at  $T_G \geq 275^\circ\text{C}$  and  $\kappa/\epsilon$ -Ga<sub>2</sub>O<sub>3</sub> at  $T_G \geq 450^\circ\text{C}$  caused a marked increase in density (Fig. 3(a)) and roughness values (Fig. 3(b)) compared to the corresponding values of amorphous films.

As can be seen in Fig. 3(a), the densities of X-ray-amorphous films did not depend on the film thickness and substrates, and showed only minor increase (from  $5.25 \pm 0.11 \text{ g cm}^{-3}$  to  $5.55 \pm 0.16 \text{ g cm}^{-3}$ ) with the  $T_G$  increase from 150 to 400 °C.

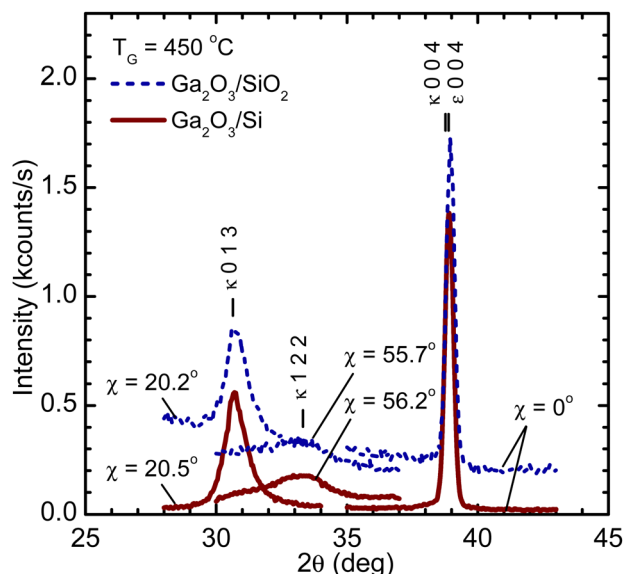


Fig. 2 Selected XRD reflections recorded in non-coplanar  $\theta$ -2 $\theta$  geometry at different inclination angles  $\chi$  for a 210 nm thick Ga<sub>2</sub>O<sub>3</sub> film grown on bare Si (solid lines) and 180 nm thick Ga<sub>2</sub>O<sub>3</sub> film grown on bare SiO<sub>2</sub> (dotted lines). The films were grown at 450 °C.





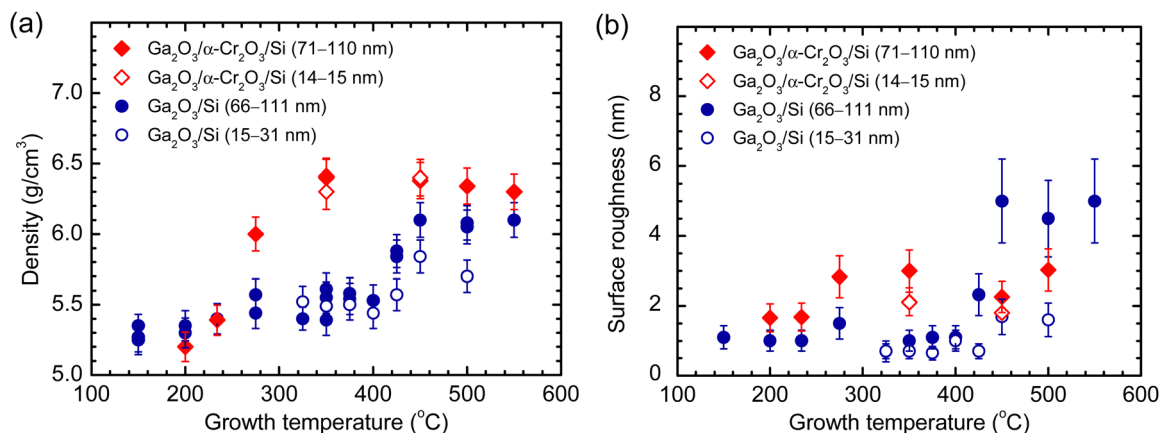


Fig. 3 (a) Density and (b) surface roughness recorded by XRR as a function of growth temperature for 14–15 nm and 71–110 nm thick  $\text{Ga}_2\text{O}_3$  films grown on  $\alpha\text{-Cr}_2\text{O}_3/\text{Si}$  substrates, and for 15–31 nm and 66–111 nm thick  $\text{Ga}_2\text{O}_3$  films grown on bare Si substrates. The thicknesses of  $\alpha\text{-Cr}_2\text{O}_3$  seed layers were  $9 \pm 3$  nm.

In contrast, the densities of films containing  $\kappa/\epsilon\text{-Ga}_2\text{O}_3$  formed on bare Si substrates at 450–550  $^{\circ}\text{C}$  were 5.93–6.10  $\text{g cm}^{-3}$ , while those of the  $\alpha\text{-Ga}_2\text{O}_3$  films obtained on the  $\alpha\text{-Cr}_2\text{O}_3/\text{Si}$  substrates at 350–550  $^{\circ}\text{C}$  reached 6.40  $\text{g cm}^{-3}$  (Fig. 3(a)). Notably, the densities recorded for the  $\alpha\text{-Ga}_2\text{O}_3$  and 66–111 nm thick  $\kappa/\epsilon\text{-Ga}_2\text{O}_3$  films were very close to the corresponding values calculated from the crystal structure parameters (6.11  $\text{g cm}^{-3}$  for  $\kappa\text{-Ga}_2\text{O}_3$  and 6.47  $\text{g cm}^{-3}$  for  $\alpha\text{-Ga}_2\text{O}_3$ ), and reported in the XRD database (PDF-2 files 01-074-1610 and 01-082-3196) and earlier papers.<sup>40,41</sup> Somewhat lower densities were determined for thinner (15–31 nm) films deposited on the bare Si substrates (Fig. 3(a)) at temperatures enabling growth of  $\kappa/\epsilon\text{-Ga}_2\text{O}_3$  (Fig. 1(a)). This result is in agreement with the results of earlier GIXRD studies<sup>44</sup> and indicates that on bare Si substrates, the growth started with formation of amorphous or another low-density phase whereas the  $\kappa/\epsilon\text{-Ga}_2\text{O}_3$  phase gradually developed with increasing film thickness. In contrast, the densities close to the XRD database values of  $\alpha\text{-Ga}_2\text{O}_3$  were obtained even for 14–15 nm films deposited on  $\alpha\text{-Cr}_2\text{O}_3/\text{Si}$  substrates at temperatures allowing crystallization of  $\text{Ga}_2\text{O}_3$  on these substrates. Consequently, on these substrates, the growth of  $\alpha\text{-Ga}_2\text{O}_3$  started from the very beginning of deposition as it can also be concluded from the data of GIXRD studies described in our previous work.<sup>44</sup>

The growth of  $\kappa/\epsilon\text{-Ga}_2\text{O}_3$  caused more significant surface roughening than the growth of  $\alpha\text{-Ga}_2\text{O}_3$  did (Fig. 3(b)). The relatively small roughness increase related to the growth of  $\alpha\text{-Ga}_2\text{O}_3$  was evidently due to the uniform nucleation of this phase on  $\alpha\text{-Cr}_2\text{O}_3$ . On the other hand, high roughness values and strong dependence of roughness on the film thickness, observed for the  $\kappa/\epsilon\text{-Ga}_2\text{O}_3$  films (Fig. 3(b)), were probably related to low concentration of nucleation centres on the bare Si substrates and faster growth of  $\kappa/\epsilon\text{-Ga}_2\text{O}_3$  compared to that of amorphous phase and different growth rates of crystallites with different orientations.

The results depicted in Fig. 4 confirm the conclusion about the faster growth of  $\kappa/\epsilon\text{-Ga}_2\text{O}_3$  compared to that of the amorphous phase. Fig. 4 clearly demonstrates that the growth per cycle (GPC) determined for films deposited with 600–700 ALD

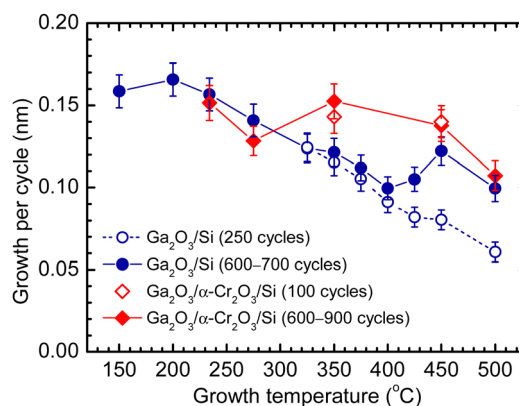


Fig. 4 Growth per cycle as a function of growth temperature for  $\text{Ga}_2\text{O}_3$  films grown with 250 and 600–700 ALD cycles on bare Si substrates and with 100 and 600–900 ALD cycles on  $\alpha\text{-Cr}_2\text{O}_3/\text{Si}$  substrates. The thicknesses of  $\alpha\text{-Cr}_2\text{O}_3$  seed layers were  $9 \pm 3$  nm.

cycles markedly increased, when  $T_G$  increased from 400 to 450  $^{\circ}\text{C}$  causing transition from the growth of amorphous phase to that of  $\kappa/\epsilon\text{-Ga}_2\text{O}_3$  (Fig. 1(a)). Interestingly, this kind of change in GPC was not observed in the case of markedly thinner films grown with 250 ALD cycles (Fig. 4). Considering the density (Fig. 3(a)) and surface roughness (Fig. 3(b)) values as well as the results of GIXRD studies reported earlier,<sup>44</sup> it was possible to conclude that the crystal structure was less developed in the films grown on bare Si with 250 ALD cycles than that in the corresponding films grown with 600–700 ALD cycles.

Notably, the  $T_G$  increase from 275 to 350  $^{\circ}\text{C}$ , causing considerable improvement in crystallinity of the films deposited on  $\alpha\text{-Cr}_2\text{O}_3$  also led to increase in GPC (Fig. 4). Therefore, the GPC of  $\alpha\text{-Ga}_2\text{O}_3$  was also higher than that of amorphous  $\text{Ga}_2\text{O}_3$ . However, no effect of the film thickness on GPC was observed in this case. As can be seen in Fig. 4, the GPC values of films grown with 100 ALD cycles on  $\alpha\text{-Cr}_2\text{O}_3$  were very close to the GPC values of films grown with 600–900 cycles on these substrates. This result confirms the conclusion about uniform



nucleation of  $\alpha$ -Ga<sub>2</sub>O<sub>3</sub> on  $\alpha$ -Cr<sub>2</sub>O<sub>3</sub> that is obviously related to epitaxial growth of  $\alpha$ -Ga<sub>2</sub>O<sub>3</sub> on  $\alpha$ -Cr<sub>2</sub>O<sub>3</sub>.

In the  $T_G$  ranges, where no transitions from amorphous to crystal growth were observed, the growth per cycle decreased with increasing  $T_G$ . This kind of decrease in GPC can be caused by an increase in the I/Ga atomic ratio in the surface species formed during GaI<sub>3</sub> adsorption. According to the results of a previous study,<sup>44</sup> this ratio was as small as 0.7 at  $T_G = 200$  °C. Therefore, the possible I/Ga increase of up to 3 could lead to a marked increase in the steric hindrance of Ga adsorption and, correspondingly, to a significantly smaller amount of Ga<sub>2</sub>O<sub>3</sub> formed during an ALD cycle. A possible reason for the increase in the I/Ga ratio is the re-adsorption of gaseous I<sub>2</sub>, formed during the adsorption of GaI<sub>3</sub>. As discussed in an earlier publication,<sup>55</sup> the re-adsorption of gaseous reaction products can explain the decrease in GPC as well as the thickness gradients that are similar to those observed in the case of films deposited from GaI<sub>3</sub> and O<sub>3</sub> at  $T_G \geq 450$  °C.<sup>44</sup> In contrast, at the precursor pulse durations used in our experiments, a considerable contribution of the thermal decomposition of GaI<sub>3</sub> to the formation of thickness gradients was unlikely at temperatures of up to 500 °C because the precursor pulse duration increase from 2 to 5 s caused marked reduction in thickness gradients but no considerable increase in GPC in the substrate areas that were close to the outlet of the precursor supply line. Simulations of chemical reactions with the HSC Chemistry 7.0 software (Outotec Research Oy), indicating that significant thermal decomposition of GaI<sub>3</sub> could start at temperatures exceeding 500–550 °C, confirmed this conclusion.

### 3.3. Optical properties

Absorption spectra of Ga<sub>2</sub>O<sub>3</sub> films grown on SiO<sub>2</sub> and  $\alpha$ -Cr<sub>2</sub>O<sub>3</sub>/SiO<sub>2</sub> substrates were calculated from transmission (Fig. 5(a)) and reflection (Fig. 5(b)) spectra. The transmission spectra (Fig. 5(a)) as well as the absorption spectra (Fig. 6(a)) demonstrate that the films were transparent or weakly absorbing at the wavelengths down to 290 nm and  $h\nu$  values of up to 4.3 eV,

approximately. The decrease in the intensities of transmission maxima observed with decreasing wavelength in this range was evidently related to the contribution of light scattering caused by the surface roughness and material inhomogeneities. According to XRR analysis, the surface roughness values of these films exceeded 5–6 nm. This kind of roughness was estimated to be sufficient to explain the transmission decrease observed at wavelengths down to 290–300 nm. This decrease in the transmission resulted in the modest increase in the absorption coefficient determined at  $h\nu$  values of up to 4.2–4.4 eV for films grown on bare SiO<sub>2</sub> and of up to 4.9 eV for a film grown on the  $\alpha$ -Cr<sub>2</sub>O<sub>3</sub>/SiO<sub>2</sub> substrate (Fig. 6(a)).

Expectedly, the absorption spectra depended on the phase composition of Ga<sub>2</sub>O<sub>3</sub> (Fig. 6(a)). The absorption onset of amorphous films deposited on SiO<sub>2</sub> at  $T_G = 310$  °C was observed at markedly lower  $h\nu$  values than those of  $\kappa/\epsilon$ -Ga<sub>2</sub>O<sub>3</sub> deposited on SiO<sub>2</sub> at 450–500 °C and, particularly, that of  $\alpha$ -Ga<sub>2</sub>O<sub>3</sub> grown on  $\alpha$ -Cr<sub>2</sub>O<sub>3</sub>/SiO<sub>2</sub> at 500 °C (Fig. 6(a)). In the absorption spectrum of  $\alpha$ -Ga<sub>2</sub>O<sub>3</sub>, two-step onset of absorption, causing a feature at 5.5–5.6 eV, was recorded (Fig. 6(a)). A similar feature, has been observed in earlier studies of  $\alpha$ -Ga<sub>2</sub>O<sub>3</sub><sup>36–39</sup> as well as monoclinic ZrO<sub>2</sub><sup>56</sup> and HfO<sub>2</sub>.<sup>53,57</sup> In all three cases, contribution of excitonic effects and specific electron band structures of these materials have been considered as possible reasons for this kind of feature.<sup>36–39,56,57</sup> For instance, in the case of  $\alpha$ -Ga<sub>2</sub>O<sub>3</sub>, an exciton band peaking at 5.5–5.6 eV and two different bandgap energies (5.61–5.62 and 6.18–6.52 eV) have been applied to fit the experimental curve recorded for the ordinary beam.<sup>38,39</sup> Notably, the absorption onsets that appeared at around 5.1 and 5.8 eV in the absorption spectra of our  $\alpha$ -Ga<sub>2</sub>O<sub>3</sub> films coincided with those reported by Segura *et al.*,<sup>37</sup> Kracht *et al.*<sup>38</sup> and Feneberg *et al.*<sup>39</sup> indicating that the bandgap energies of these films were very similar to each other.

However, in a number of applications, the performance of  $\alpha$  at the optical absorption edge rather than in the range of strong absorption is of importance. Therefore, the  $E_g$  values are frequently determined from the  $(\alpha h\nu)^2$  versus  $h\nu$  or  $(\alpha h\nu)^{1/2}$

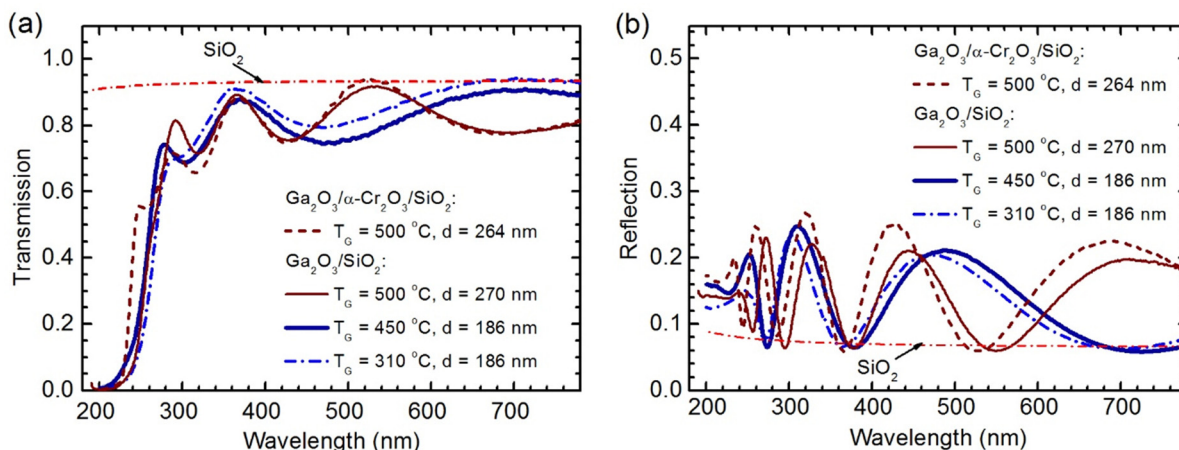


Fig. 5 Optical (a) transmission and (b) reflection spectra of Ga<sub>2</sub>O<sub>3</sub> films grown at different temperatures on SiO<sub>2</sub> and  $\alpha$ -Cr<sub>2</sub>O<sub>3</sub>/SiO<sub>2</sub> substrates. The thickness of the  $\alpha$ -Cr<sub>2</sub>O<sub>3</sub> layer was  $1.1 \pm 0.4$  nm.



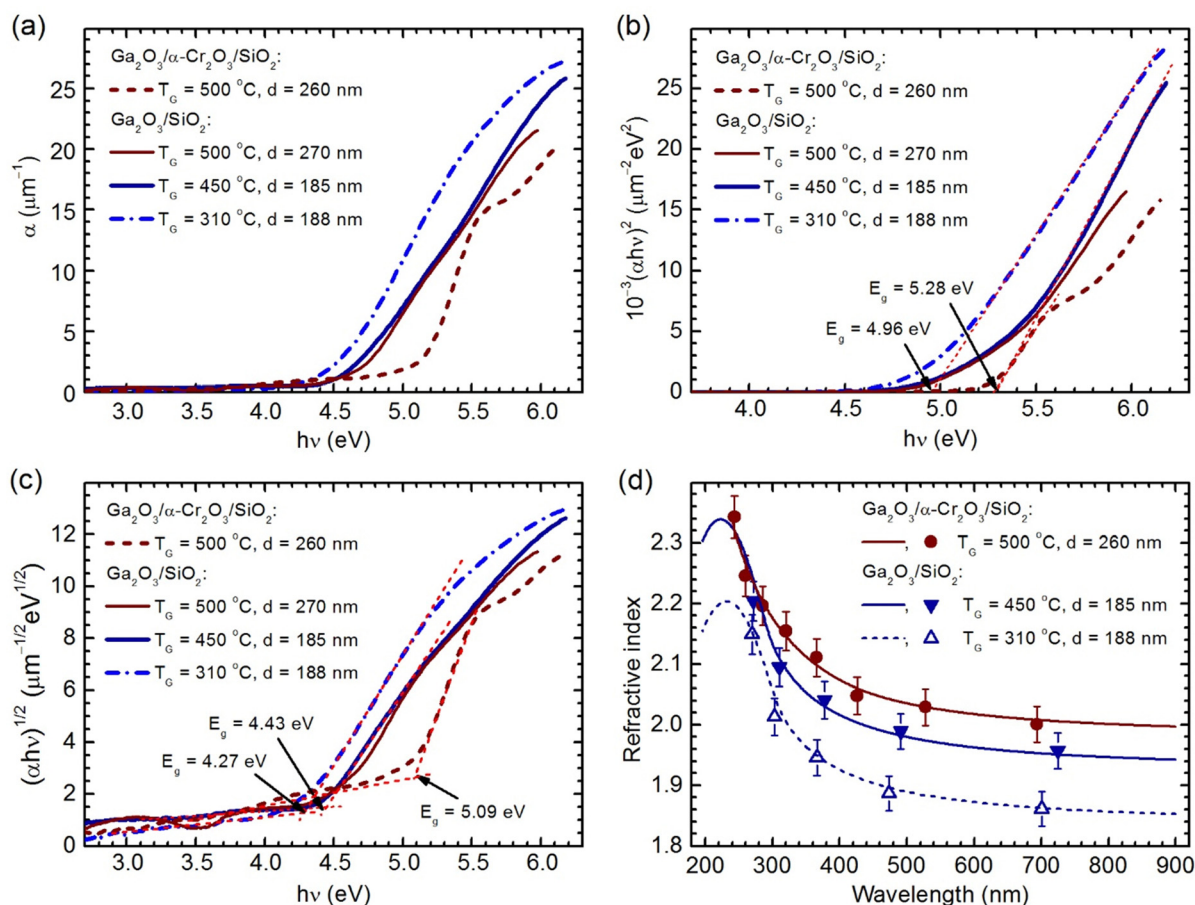


Fig. 6 (a) Absorption coefficient, (b)  $(\alpha h\nu)^2$ , and (c)  $(\alpha h\nu)^{1/2}$  as a function of  $h\nu$ , and (d) refractive index as a function of wavelength determined for  $\text{Ga}_2\text{O}_3$  films grown at different temperatures on  $\text{SiO}_2$  and  $\alpha\text{-Cr}_2\text{O}_3/\text{SiO}_2$  substrates. The thickness of the  $\alpha\text{-Cr}_2\text{O}_3$  layer was  $1.1 \pm 0.4$  nm.

versus  $h\nu$  plots, while the former plots assuming direct optical transitions have mainly been used to determine optical bandgap energies of  $\alpha\text{-Ga}_2\text{O}_3$ ,<sup>20,26,32–35</sup>  $\epsilon\text{-Ga}_2\text{O}_3$ ,<sup>45,46</sup>  $\kappa\text{-Ga}_2\text{O}_3$ ,<sup>9,47</sup> and amorphous  $\text{Ga}_2\text{O}_3$ .<sup>13–15,17,18,20,21,23–26</sup> Extrapolating the linear parts of the  $(\alpha h\nu)^2$  versus  $h\nu$  plots of our films (Fig. 5(b)) yielded the optical bandgap energies in the approximation of direct optical transitions ( $E_{\text{dg}}$ ) at 4.96 eV for amorphous  $\text{Ga}_2\text{O}_3$ , 5.22–5.28 eV for  $\kappa/\epsilon\text{-Ga}_2\text{O}_3$ , and 5.28 eV for  $\alpha\text{-Ga}_2\text{O}_3$  (Table 1). The  $E_{\text{dg}}$  values of amorphous  $\text{Ga}_2\text{O}_3$  and  $\alpha\text{-Ga}_2\text{O}_3$  were consistent with corresponding values of 4.05–5.47 eV<sup>13–15,17,18,20,21,23–26</sup> and 5.04–5.36 eV<sup>20,26,32–35</sup> reported in earlier publications. In contrast, the  $E_{\text{dg}}$  values determined for  $\kappa/\epsilon\text{-Ga}_2\text{O}_3$  exceeded those of 4.6–5 eV<sup>45,46</sup> and 4.9–5.14 eV<sup>9,29,47,48</sup> published for  $\epsilon\text{-Ga}_2\text{O}_3$  and  $\kappa\text{-Ga}_2\text{O}_3$ , respectively. It is also worth mentioning that  $E_{\text{dg}}$  obtained for our amorphous  $\text{Ga}_2\text{O}_3$  films were very close to the most typical values of 4.80–5.00 eV obtained for amorphous  $\text{Ga}_2\text{O}_3$  films grown by ALD previously.<sup>13–16,18,24</sup>

Comparing the absorption spectra (Fig. 6(a)) and  $E_{\text{dg}}$  values obtained from the results depicted in Fig. 6(b), one can see that the absorption was relatively strong at the  $E_{\text{dg}}$  values determined from the  $(\alpha h\nu)^2$  versus  $h\nu$  curves. Consequently, the direct transition analysis was not sensitive enough to the absorption at the photon energies close to the absorption edges

Table 1 Optical bandgap values  $E_{\text{dg}}$  determined from the  $(\alpha h\nu)^2$  versus  $h\nu$  plots and  $E_{\text{ig}}$  determined from the  $(\alpha h\nu)^{1/2}$  versus  $h\nu$  plots for 185–270 nm thick  $\text{Ga}_2\text{O}_3$  films grown on  $\text{SiO}_2$  and  $\alpha\text{-Cr}_2\text{O}_3/\text{SiO}_2$  substrates

$T_{\text{G}}$ (°C)	Substrate	$d$ (nm)	Phase	$E_{\text{dg}}$ (eV)	$E_{\text{ig}}$ (eV)
310	$\text{SiO}_2$	188	Amorphous	$4.96 \pm 0.03$	$4.27 \pm 0.03$
450	$\text{SiO}_2$	185	$\kappa/\epsilon\text{-Ga}_2\text{O}_3$	$5.28 \pm 0.03$	$4.43 \pm 0.03$
500	$\text{SiO}_2$	270	$\kappa/\epsilon\text{-Ga}_2\text{O}_3$	$5.22 \pm 0.05$	$4.43 \pm 0.04$
500	$\alpha\text{-Cr}_2\text{O}_3/\text{SiO}_2^a$	260	$\alpha\text{-Ga}_2\text{O}_3$	$5.28 \pm 0.03$	$5.09 \pm 0.03$

<sup>a</sup> The thickness of the  $\alpha\text{-Cr}_2\text{O}_3$  layer was  $1.1 \pm 0.4$  nm.

of these materials. Furthermore, the linear parts in the  $(\alpha h\nu)^2$  versus  $h\nu$  plots of the films deposited on  $\text{SiO}_2$  at 450–500 °C were relatively short and appeared at photon energies significantly exceeding the  $E_{\text{dg}}$  values determined from these plots (Fig. 6(b)). This obviously resulted in additional uncertainty in the determination of  $E_{\text{dg}}$  for these films. Therefore, the optical bandgap energies were also determined from the  $(\alpha h\nu)^{1/2}$  versus  $h\nu$  plots (Fig. 6(c)) assuming indirect optical transitions between the valence and conduction bands. The  $E_{\text{ig}}$  values obtained in this approximation were 4.27 eV for amorphous  $\text{Ga}_2\text{O}_3$ , 4.43 eV for  $\kappa/\epsilon\text{-Ga}_2\text{O}_3$ , and 5.09 eV for  $\alpha\text{-Ga}_2\text{O}_3$  (Table 1). These energies correspond well to the absorption onsets





(Fig. 6(a)). Therefore, it is possible that the  $\text{Ga}_2\text{O}_3$  phases studied in this work have indirect bandgaps as it has been predicted for  $\alpha\text{-Ga}_2\text{O}_3$  in theoretical calculations.<sup>58–60</sup> Notably, the  $E_{\text{dg}} - E_{\text{ig}}$  value of 0.19 eV, determined from the absorption spectra of  $\alpha\text{-Ga}_2\text{O}_3$  in this work is close to the corresponding values of 0.21–0.25 eV obtained from the first-principles calculations.<sup>58–60</sup>

Alternatively, there is a possibility that the bandgap is direct but the electron transitions do not follow the momentum selection rule, when the photon energies causing the transitions are close to the bandgap energies. The latter effect might be related to the structural defects, impurities, and/or band tails that can contribute to the electron transitions at photon energies close to the bandgap values.<sup>61</sup> Therefore, it is not surprising that the recent experimental results of Ma *et al.*,<sup>62</sup> yielding an  $E_{\text{ig}}$  value of 5.02 eV for  $\alpha\text{-Ga}_2\text{O}_3$  from the  $(\alpha h\nu)^{1/2}$  versus  $h\nu$  plots, also indicate that contribution of indirect transitions to the shapes of absorption spectra at the absorption edge of this phase cannot be neglected.

Refractive indices determined as a function of wavelength for the  $\text{Ga}_2\text{O}_3$  films deposited on  $\text{SiO}_2$  and  $\alpha\text{-Cr}_2\text{O}_3/\text{SiO}_2$  substrates are depicted in Fig. 6(d). The experimental points with error bars correspond to the  $n$  values determined from the spectrophotometry data, while the curves were calculated from the results of SE measurements. Expectedly, the  $n$  values of  $\kappa/\epsilon\text{-Ga}_2\text{O}_3$  and  $\alpha\text{-Ga}_2\text{O}_3$  films grown on  $\text{SiO}_2$  and  $\alpha\text{-Cr}_2\text{O}_3/\text{SiO}_2$  at 450 and 500 °C, respectively, were markedly higher than those of an amorphous film deposited on  $\text{SiO}_2$  at 310 °C (Fig. 6(d)). Very similar results, obtained for the 80–107 nm thick films on Si and  $\alpha\text{-Cr}_2\text{O}_3/\text{Si}$ , are shown in Fig. 7.

The data presented in Fig. 7 demonstrate that the variation of  $T_{\text{G}}$  from 200 to 375 °C and from 450 to 550 °C did not cause considerable changes in the  $n$  values and dispersion curves of the films grown on Si substrates. However, the  $T_{\text{G}}$  increase from 375 to 450 °C causing the transition from the growth of

**Table 2** Comparison of refractive index values determined by spectroscopic ellipsometry at 365 and 633 nm for  $\text{Ga}_2\text{O}_3$  films grown on Si,  $\text{SiO}_2$ ,  $\alpha\text{-Cr}_2\text{O}_3/\text{Si}$ , and  $\alpha\text{-Cr}_2\text{O}_3/\text{SiO}_2$  substrates

$T_{\text{G}}$ (°C)	Substrate	$d$ (nm)	Phase	$n$ at 365 nm	$n$ at 633 nm
310	Si	188	Amorphous	$1.95 \pm 0.02$	$1.86 \pm 0.02$
310	$\text{SiO}_2$	188	Amorphous	$1.95 \pm 0.02$	$1.86 \pm 0.02$
450	Si	189	$\kappa/\epsilon\text{-Ga}_2\text{O}_3$	$2.01 \pm 0.03$	$1.93 \pm 0.02$
450	$\text{SiO}_2$	185	$\kappa/\epsilon\text{-Ga}_2\text{O}_3$	$2.02 \pm 0.03$	$1.94 \pm 0.02$
500	Si	273	$\kappa/\epsilon\text{-Ga}_2\text{O}_3$	$2.06 \pm 0.03$	$1.98 \pm 0.02$
500	$\text{SiO}_2$	270	$\kappa/\epsilon\text{-Ga}_2\text{O}_3$	$2.04 \pm 0.03$	$1.98 \pm 0.02$
500	$\alpha\text{-Cr}_2\text{O}_3/\text{Si}^a$	269	$\alpha\text{-Ga}_2\text{O}_3$	$2.06 \pm 0.03$	$2.01 \pm 0.03$
500	$\alpha\text{-Cr}_2\text{O}_3/\text{SiO}_2^b$	260	$\alpha\text{-Ga}_2\text{O}_3$	$2.09 \pm 0.03$	$2.02 \pm 0.03$

<sup>a</sup> The thickness of the  $\alpha\text{-Cr}_2\text{O}_3$  layer was  $0.7 \pm 0.3$  nm. <sup>b</sup> The thickness of the  $\alpha\text{-Cr}_2\text{O}_3$  layer was  $1.1 \pm 0.4$  nm.

amorphous phase to the growth of  $\kappa/\epsilon\text{-Ga}_2\text{O}_3$  led to a marked increase in  $n$  (Fig. 7). In line with the results presented in Fig. 6(d), even higher  $n$  values were measured for the  $\alpha\text{-Ga}_2\text{O}_3$  films deposited on the  $\alpha\text{-Cr}_2\text{O}_3/\text{Si}$  substrates.

As it was expected, the films grown on Si and  $\alpha\text{-Cr}_2\text{O}_3/\text{Si}$  substrates had  $n$  values that were very similar to those of the films deposited on  $\text{SiO}_2$  and  $\alpha\text{-Cr}_2\text{O}_3/\text{SiO}_2$ , respectively (Table 2). The minor differences observed did not exceed the experimental uncertainty. Comparing the results presented in Table 2 and Fig. 8, one can see that at  $d > 80$  nm, the dependence of  $n$  on  $d$  was weak. However, at lower film thicknesses,  $n$  decreased with decreasing  $d$  (Fig. 8(a)).

As an one-layer model was used to analyse the SE data, one probable reason for the decrease in  $n$  observed with decreasing  $d$  at lower film thicknesses was the increasing contribution of surface roughness, causing the formation of surface layer with lower density and, correspondingly, a decrease in the mean value of  $n$  calculated from the SE results. For instance, the XRR analysis yielded surface roughness values of 0.9 and 1.0 nm for the 59 and 85 nm thick films grown on Si at 350 °C, 4.5 and 5.0 nm for the 44 and 85 nm thick films grown on Si at 450 °C, and 2.5 nm for the 43 and 83 nm thick films grown on  $\alpha\text{-Cr}_2\text{O}_3/\text{Si}$  at 450 °C. Therefore, with the thickness decrease in these  $d$  ranges, the surface roughness decreased insignificantly or did not decrease at all. Correspondingly, the relative amount of material with lower  $n$  increased with decreasing film thickness leading to the decrease in the mean value of  $n$ .

To characterize the effect of  $T_{\text{G}}$  on  $n$  in more detail, the values of  $n$  determined at wavelengths of 365 and 633 nm for films with thicknesses of 79–107 nm deposited on Si and  $\alpha\text{-Cr}_2\text{O}_3/\text{Si}$  substrates are displayed in Fig. 8(b) as a function of  $T_{\text{G}}$ . Comparison of the results presented in Fig. 1(a), (b) and 8(b) leads to a conclusion that the effect of  $T_{\text{G}}$  on  $n$  is insignificant in the  $T_{\text{G}}$  ranges where no phase transitions take place. For instance, no considerable influence of  $T_{\text{G}}$  was observed on  $n$  of amorphous films grown on bare Si at 150–425 °C,  $\kappa/\epsilon\text{-Ga}_2\text{O}_3$  films grown on bare Si substrates at 450–550 °C, and  $\alpha\text{-Ga}_2\text{O}_3$  films grown on  $\alpha\text{-Cr}_2\text{O}_3/\text{Si}$  at 350–550 °C. In contrast, marked increase in  $n$  of films deposited on bare Si and  $\alpha\text{-Cr}_2\text{O}_3/\text{Si}$  is observed with the  $T_{\text{G}}$  increase from 425 to 450 °C and from 230 to 350 °C, respectively (Fig. 8(b)), that is,

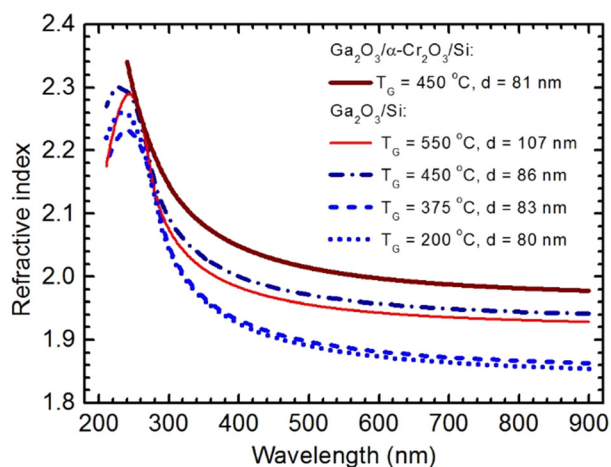


**Fig. 7** Refractive index as a function of wavelength determined by spectroscopic ellipsometry for  $\text{Ga}_2\text{O}_3$  films grown at different temperatures on Si and  $\alpha\text{-Cr}_2\text{O}_3/\text{Si}$  substrates. The thickness of the  $\alpha\text{-Cr}_2\text{O}_3$  layer was  $1.1 \pm 0.4$  nm.





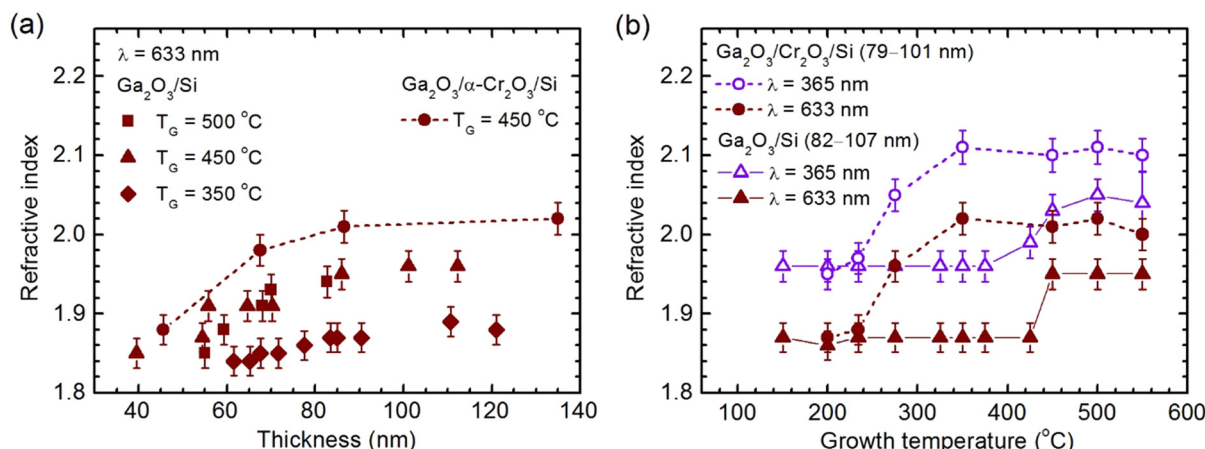


Fig. 8 Refractive index as a function of (a) thickness of films grown at 350, 450 and 500  $^\circ\text{C}$  and (b) growth temperatures of 82–107 nm thick films grown on Si and 79–101 nm thick films grown on  $\alpha\text{-Cr}_2\text{O}_3/\text{Si}$  substrates. The  $\alpha\text{-Cr}_2\text{O}_3$  seed layer thicknesses were  $9 \pm 3\text{ nm}$ . The refractive indices were calculated at wavelengths of (a) 633 nm and (b) 365 and 633 nm from the spectroscopic ellipsometry data.

with the transition from the growth of amorphous to that of crystalline films (Fig. 1(a) and (b)).

The  $n$  values, obtained for amorphous  $\text{Ga}_2\text{O}_3$  in this work (Table 2 and Fig. 8(b)), were well comparable to the highest values (1.84–1.87 at  $\lambda = 633\text{ nm}$ ) reported for amorphous films in previous ALD studies.<sup>13,14,16,18</sup> In addition, the  $n$  values obtained for the films grown on  $\alpha\text{-Cr}_2\text{O}_3/\text{Si}$  and  $\alpha\text{-Cr}_2\text{O}_3/\text{SiO}_2$  in this work (Table 2 and Fig. 8(b)) were close to a value of 2.00 that can be determined from the ellipsometry data of Feneberg *et al.*<sup>39</sup> published for the epitaxial films grown on  $\alpha\text{-Al}_2\text{O}_3$  (0 0 0 1) by ultrasonic mist chemical vapour epitaxy.

When comparing the results of our experiments with those of earlier studies, one can see that the  $n$  values of  $\kappa/\epsilon\text{-Ga}_2\text{O}_3$  films recorded at 633 nm (Table 2 and Fig. 8) are somewhat higher than the corresponding values of 1.83–1.94 at 633 nm reported for stoichiometric  $\beta\text{-Ga}_2\text{O}_3$ .<sup>14,16,22,25,27,28,30</sup> One can also notice that refractive indices of 2.00–2.02 obtained for  $\alpha\text{-Ga}_2\text{O}_3$  at 633 nm in this work (Table 2 and Fig. 8) and by

Feneberg *et al.*<sup>39</sup> are close to that of 2.04 determined at 633 nm for  $\gamma\text{-Ga}_2\text{O}_3$ .<sup>58,63</sup> However, the  $E_{\text{dg}}$  and  $E_{\text{ig}}$  values of  $\alpha\text{-Ga}_2\text{O}_3$  (Table 1) are markedly higher than the respective values of 5.0 and 4.4 eV<sup>58,63</sup> reported for  $\gamma\text{-Ga}_2\text{O}_3$ .

In agreement with theoretical considerations and results obtained earlier for other materials,<sup>64–66</sup> the refractive index values (Fig. 8) increase together with the material densities (Fig. 3(a)). Additionally, our data demonstrate that the  $E_g$  values are in positive correlation with the densities of  $\text{Ga}_2\text{O}_3$  phases studied in this work. The latter result is not common for other materials. For instance, high-density rutile and  $\text{TiO}_2\text{-II}$  phases of  $\text{TiO}_2$  have narrower bandgaps compared to that of the low-density anatase phase.<sup>66</sup> An explanation for this difference can be deduced from the results of Ohta *et al.*,<sup>67</sup> who investigated phase transition of anatase to  $\text{TiO}_2\text{-II}$  at high hydrostatic pressures. They observed a predictable shift of the optical absorption edge of anatase to higher energies, caused by the reduction of average bond length and corresponding increase

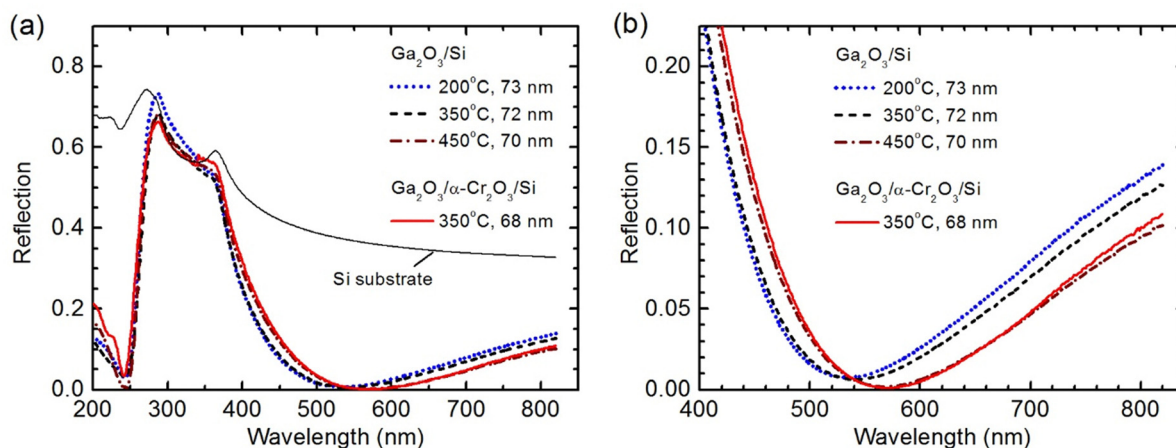


Fig. 9 Reflection spectra recorded in wavelength ranges of (a) 200–820 nm and (b) 400–820 nm for silicon substrates coated with  $\text{Ga}_2\text{O}_3$  and  $\text{Ga}_2\text{O}_3/\alpha\text{-Cr}_2\text{O}_3$  antireflection coatings. (a) Reflection spectrum of bare silicon substrate is shown for comparison. The thickness of  $\alpha\text{-Cr}_2\text{O}_3$  was  $1.5 \pm 0.5\text{ nm}$ .



**Table 3** Properties of Ga<sub>2</sub>O<sub>3</sub> and Ga<sub>2</sub>O<sub>3</sub>/α-Cr<sub>2</sub>O<sub>3</sub> antireflection coatings deposited on Si substrates

$T_G$ (°C)	Phase	Thickness (nm)	$\lambda_{\min}$ (nm)	$R_{\min}$ (%)
200	Amorphous	73 ± 3	533 ± 5	0.75 ± 0.08
350	Amorphous	72 ± 3	540 ± 5	0.68 ± 0.07
450	κ/ε-Ga <sub>2</sub> O <sub>3</sub>	70 ± 3	570 ± 5	0.20 ± 0.05
350	α-Ga <sub>2</sub> O <sub>3</sub> /α-Cr <sub>2</sub> O <sub>3</sub>	68 ± 3/1.5 ± 0.5	570 ± 5	0.12 ± 0.04

in the material density under the increasing hydrostatic pressure. However, at pressures causing the phase transformation from anatase to TiO<sub>2</sub>-II, an abrupt absorption-spectrum shift to lower energies appeared because of the atomic rearrangement. Therefore, the higher  $E_g$  values, recorded for Ga<sub>2</sub>O<sub>3</sub> phases with higher densities in our experiments, indicate that the differences of the atomic arrangements in these phases from those in the Ga<sub>2</sub>O<sub>3</sub> phases with lower densities do not cause bandgap shrinking that would be comparable to the  $E_g$  increase due to the decrease in the average bond length or unit cell volume.<sup>60,68</sup>

In the visible range of spectrum, the  $n^2$  values calculated on the basis of data depicted in Table 2 and Fig. 8 were close to the refractive index value of silicon.<sup>69</sup> Therefore, the Ga<sub>2</sub>O<sub>3</sub> films studied in this work were expected to be suitable for highly efficient single-layer antireflection (AR) coatings of silicon-based optoelectronic devices, for instance, solar cells and photodiodes. The reflection spectra, measured for silicon substrates coated with Ga<sub>2</sub>O<sub>3</sub> and Ga<sub>2</sub>O<sub>3</sub>/α-Cr<sub>2</sub>O<sub>3</sub> thin films at different temperatures, demonstrate that at wavelengths ( $\lambda_{\min}$ ) corresponding to the reflection minima, the reflection values ( $R_{\min}$ ) below 1% can be obtained for all coatings studied (Fig. 9 and Table 3). The lowest  $R_{\min}$  values that reached 0.12% were recorded for the α-Ga<sub>2</sub>O<sub>3</sub>/α-Cr<sub>2</sub>O<sub>3</sub> AR coatings. However, the  $R_{\min}$  of the κ/ε-Ga<sub>2</sub>O<sub>3</sub>-coated Si was also very low (Table 3).

It is also worth noting that the light transmission through the α-Ga<sub>2</sub>O<sub>3</sub>/α-Cr<sub>2</sub>O<sub>3</sub> AR coatings is sufficiently high only at wavelengths exceeding 400 nm. At lower wavelengths, the absorption of light in the α-Cr<sub>2</sub>O<sub>3</sub> seed layer might become significant. For instance, using the data published for α-Cr<sub>2</sub>O<sub>3</sub> thin films,<sup>70</sup> the absorption in a 1 nm thick seed layer was estimated to increase from ≤0.2% at 400 nm to 1.5% at 350 nm, 3.8% at 300 nm, and 8% at 200 nm. Hence at wavelengths below 400 nm, the κ/ε-Ga<sub>2</sub>O<sub>3</sub>-AR coatings are evidently more efficient than the α-Ga<sub>2</sub>O<sub>3</sub>/α-Cr<sub>2</sub>O<sub>3</sub> AR coatings.

## 4. Conclusions

The results of this work confirm significant influence of the crystal growth and phase composition on the density and optical properties of Ga<sub>2</sub>O<sub>3</sub>. Notably the formation of phases with higher densities caused an increase in both the optical bandgap energies and refractive indices. The bandgap energies, estimated from the  $(\alpha h\nu)^2$  versus  $h\nu$  plots for the amorphous, κ/ε, and α phases of Ga<sub>2</sub>O<sub>3</sub> with the densities of 5.2–5.6, 5.9–6.1, and 6.2–6.4 g cm<sup>-3</sup>, were 4.96, 5.22–5.28, and 5.28 eV, respectively. These values were consistent with previous data, obtained using the same approach that assumed domination of

direct optical transitions in the absorption process. However, the bandgap values of 4.27, 4.43, and 5.09 eV, respectively, determined from the  $(\alpha h\nu)^{1/2}$  versus  $h\nu$  plots corresponding to the indirect transitions, characterized the optical absorption edge energies even better. This result indicates that most probably, the electron transitions, caused by absorption of radiation with photon energies close to the absorption edge, do not follow the momentum selection rule although most of the Ga<sub>2</sub>O<sub>3</sub> phases have generally been considered to be direct bandgap materials. Influence of impurities and/or structural defects on optical transitions can be a possible reason for this effect. The refractive index values of amorphous Ga<sub>2</sub>O<sub>3</sub>, κ/ε-Ga<sub>2</sub>O<sub>3</sub>, and α-Ga<sub>2</sub>O<sub>3</sub> films, measured at 633 nm for films with thicknesses exceeding 70 nm, were 1.86 ± 0.03, 1.96 ± 0.03 and 2.01 ± 0.02, respectively. Because of appropriate refractive index values, these Ga<sub>2</sub>O<sub>3</sub> phases appeared to be suitable for applications in AR coatings allowing the reduction of reflection from the silicon surface down to 0.12–0.20%.

The results of this work also reveal that the crystallization processes markedly influence GPC. Moreover, on the substrates that do not support epitaxial growth of a crystalline phase, the spontaneous crystallization may lead to considerable dependence of GPC on the Ga<sub>2</sub>O<sub>3</sub> film thickness. These effects should also be considered when designing ALD processes for the deposition of optical coatings because, as a rule, the thickness is an important parameter of a thin film deposited for optical applications.

## Data availability

Data are available upon request from the authors.

## Conflicts of interest

There are no conflicts to declare.

## Acknowledgements

The authors are grateful to Alma-Asta Kiisler and Peeter Ritslaid for technical assistance. The research was funded by the Estonian Research Council (grants PSG448 and PRG753).

## References

- S. J. Pearton, F. Ren, M. Tadjer and J. Kim, Perspective: Ga<sub>2</sub>O<sub>3</sub> for ultra-high power rectifiers and MOSFETS, *J. Appl. Phys.*, 2018, **124**, 220901, DOI: [10.1063/1.5062841](https://doi.org/10.1063/1.5062841).
- J.-S. Li, C.-C. Chiang, X. Xia, T. J. Yoo, F. Ren, H. Kim and S. J. Pearton, Demonstration of 4.7 kV breakdown voltage in NiO/β-Ga<sub>2</sub>O<sub>3</sub> vertical rectifiers, *Appl. Phys. Lett.*, 2022, **121**, 042105, DOI: [10.1063/5.0097564](https://doi.org/10.1063/5.0097564).
- A.-C. Liu, C.-H. Hsieh, C. Langpoklakpam, K. J. Singh, W.-C. Lee, Y.-K. Hsiao, R.-H. Horng, H.-C. Kuo and C.-C. Tu, State-of-the-art β-Ga<sub>2</sub>O<sub>3</sub> field effect transistors for



- power electronics, *ACS Omega*, 2022, **7**, 36070–36091, DOI: [10.1021/acsomega.2c03345](https://doi.org/10.1021/acsomega.2c03345).
- 4 J. Wang, H. Guo, C.-Z. Zhu, Q. Cai, G.-F. Yang, J.-J. Xue, D.-J. Chen, Y. Tong, B. Liu, H. Lu, R. Zhang and Y.-D. Zheng,  $\epsilon$ -Ga<sub>2</sub>O<sub>3</sub>: a promising candidate for high-electron-mobility transistors, *IEEE Electron Device Lett.*, 2020, **41**, 1052–1055, DOI: [10.1109/LED.2020.2995446](https://doi.org/10.1109/LED.2020.2995446).
  - 5 Z. Yang, J. Wu, P. Li, Y. Chen, Y. Yan, B. Zhu, C. S. Hwang, W. Mi, J. Zhao, K. Zhang and R. Guo, Resistive random access memory based on gallium oxide thin films for self-powered pressure sensor systems, *Ceram. Int.*, 2020, **46**, 21141–21148, DOI: [10.1016/j.ceramint.2020.05.191](https://doi.org/10.1016/j.ceramint.2020.05.191).
  - 6 X. Li, J.-G. Yang, H.-P. Ma, Y.-H. Liu, Z.-G. Ji, W. Huang, X. Ou, D. W. Zhang and H.-L. Lu, Atomic layer deposition of Ga<sub>2</sub>O<sub>3</sub>/ZnO composite films for high-performance forming-free resistive switching memory, *ACS Appl. Mater. Interfaces*, 2020, **12**, 30538–30547, DOI: [10.1021/acsami.0c06476](https://doi.org/10.1021/acsami.0c06476).
  - 7 M. Pavesi, F. Fabbri, F. Boschi, G. Piacentini, A. Baraldi, M. Bosi, E. Gombia, A. Parisini and R. Fornari,  $\epsilon$ -Ga<sub>2</sub>O<sub>3</sub> epilayers as a material for solar-blind UV photodetectors, *Mater. Chem. Phys.*, 2018, **205**, 502–507, DOI: [10.1016/j.matchemphys.2017.11.023](https://doi.org/10.1016/j.matchemphys.2017.11.023).
  - 8 H. Qian, X. Zhang, Y. Ma, L. Zhang, T. Chen, X. Wei, W. Tang, X. Zhou, B. Feng, Y. Fan, Y. Sun and B. Zhang, Quasi-vertical  $\epsilon$ -Ga<sub>2</sub>O<sub>3</sub> solar blind photodetectors grown on p-Si substrates with Al<sub>2</sub>O<sub>3</sub> buffer layer by metalorganic chemical vapor deposition, *Vacuum*, 2022, **200**, 111019, DOI: [10.1016/j.vacuum.2022.111019](https://doi.org/10.1016/j.vacuum.2022.111019).
  - 9 N. Lim, J. Min, J.-H. Min, C. H. Kang, K.-H. Li, T.-Y. Park, W. Kim, B. Davaasuren, T. K. Ng, B. S. Ooi, D. H. Woo, J.-H. Park and Y. Pak, Ultrasensitive UV-C detection based on MOCVD-grown highly crystalline ultrawide bandgap orthorhombic  $\kappa$ -Ga<sub>2</sub>O<sub>3</sub>, *Appl. Surf. Sci.*, 2023, **609**, 155350, DOI: [10.1016/j.apsusc.2022.155350](https://doi.org/10.1016/j.apsusc.2022.155350).
  - 10 J. Blevins and G. Yang, On optical properties and scintillation performance of emerging Ga<sub>2</sub>O<sub>3</sub>: crystal growth, emission mechanisms and doping strategies, *Mater. Res. Bull.*, 2021, **144**, 111494, DOI: [10.1016/j.materresbull.2021.111494](https://doi.org/10.1016/j.materresbull.2021.111494).
  - 11 L. I. Guzilova, A. S. Gershchenko, P. N. Butenko, A. V. Chikiryaka, A. I. Pechnikov and V. I. Nikolaev, Mechanical properties of epilayers of metastable  $\alpha$ - and  $\epsilon$ -Ga<sub>2</sub>O<sub>3</sub> phases studied by nanoindentation, *Tech. Phys. Lett.*, 2021, **47**, 709–713, DOI: [10.1134/S106378502107021X](https://doi.org/10.1134/S106378502107021X).
  - 12 A. K. Battu and C. V. Ramana, Mechanical properties of nanocrystalline and amorphous gallium oxide thin films, *Adv. Eng. Mater.*, 2018, **20**, 1701033, DOI: [10.1002/adem.201701033](https://doi.org/10.1002/adem.201701033).
  - 13 D. Hiller, J. Julin, A. Chnani and S. Strehle, Silicon surface passivation by ALD-Ga<sub>2</sub>O<sub>3</sub>: thermal vs. plasma-enhanced atomic layer deposition, *IEEE J. Photovolt.*, 2020, **10**, 959–968, DOI: [10.1109/JPHOTOV.2020.2989201](https://doi.org/10.1109/JPHOTOV.2020.2989201).
  - 14 F. K. Shan, G. X. Liu, W. J. Lee, G. H. Lee, I. S. Kim and B. C. Shin, Structural, electrical, and optical properties of transparent gallium oxide thin films grown by plasma-enhanced atomic layer deposition, *J. Appl. Phys.*, 2005, **98**, 023504, DOI: [10.1063/1.1980535](https://doi.org/10.1063/1.1980535).
  - 15 D. J. Comstock and J. W. Elam, Atomic layer deposition of Ga<sub>2</sub>O<sub>3</sub> films using trimethylgallium and ozone, *Chem. Mater.*, 2012, **24**, 4011–4018, DOI: [10.1021/cm300712x](https://doi.org/10.1021/cm300712x).
  - 16 R. K. Ramachandran, J. Dendooven, J. Botterman, S. Pulinthanathu Sree, D. Poelman, J. A. Martens, H. Poelman and C. Detavernier, Plasma enhanced atomic layer deposition of Ga<sub>2</sub>O<sub>3</sub> thin films, *J. Mater. Chem.*, 2014, **A2**, 19232–19238, DOI: [10.1039/C4TA05007J](https://doi.org/10.1039/C4TA05007J).
  - 17 A. Mahmoodinezhad, C. Janowitz, F. Naumann, P. Plate, H. Gargouri, K. Henkel, D. Schmeißer and J. I. Flege, Low-temperature growth of gallium oxide thin films by plasma-enhanced atomic layer deposition, *J. Vac. Sci. Technol., A*, 2020, **38**, 022404, DOI: [10.1116/1.5134800](https://doi.org/10.1116/1.5134800).
  - 18 H. Kröncke, F. Maudet, S. Banerjee, J. Albert, S. Wiesner, V. Deshpande and C. Dubourdieu, Effect of plasma exposure time during atomic layer deposition of amorphous gallium oxide, *J. Vac. Sci. Technol., A*, 2021, **39**, 052408, DOI: [10.1116/6.0001207](https://doi.org/10.1116/6.0001207).
  - 19 B. R. Tak, S. Kumar, A. K. Kapoor, D. Wang, X. Li, H. Sun and R. Singh, Recent advances in the growth of gallium oxide thin films employing various growth techniques—a review, *J. Phys. D: Appl. Phys.*, 2021, **54**, 453002, DOI: [10.1088/1361-6463/ac1af2](https://doi.org/10.1088/1361-6463/ac1af2).
  - 20 V. Gottschalch, S. Merker, S. Blaurock, M. Kneiß, U. Teschner, M. Grundmann and H. Krautscheid, Hetero-epitaxial growth of  $\alpha$ -,  $\beta$ -,  $\gamma$ - and  $\kappa$ -Ga<sub>2</sub>O<sub>3</sub> phases by metalorganic vapor phase epitaxy, *J. Cryst. Growth*, 2019, **510**, 76–84, DOI: [10.1016/j.jcrysgro.2019.01.018](https://doi.org/10.1016/j.jcrysgro.2019.01.018).
  - 21 M. F. Al-Kuhaili, S. M. A. Durrani and E. E. Khawaja, Optical properties of gallium oxide films deposited by electron-beam evaporation, *Appl. Phys. Lett.*, 2003, **83**, 4533, DOI: [10.1063/1.1630845](https://doi.org/10.1063/1.1630845).
  - 22 F. K. Shan, G. X. Liu, W. J. Lee, I. S. Kim and B. C. Shin, Ga<sub>2</sub>O<sub>3</sub> thin film deposited by atomic layer deposition with high plasma power, *Integr. Ferroelectr.*, 2006, **80**, 197–206, DOI: [10.1080/10584580600657666](https://doi.org/10.1080/10584580600657666).
  - 23 G. X. Liu, F. K. Shan, W. J. Lee, B. C. Shin, S. C. Kim, H. S. Kim and C. R. Cho, Growth temperature dependence of Ga<sub>2</sub>O<sub>3</sub> thin films deposited by plasma enhanced atomic layer deposition, *Integr. Ferroelectr.*, 2007, **94**, 11–20, DOI: [10.1080/1058458070175571](https://doi.org/10.1080/1058458070175571).
  - 24 R. O'Donoghue, J. Rechmann, M. Aghaee, D. Rogalla, H. W. Becker, M. Creatore, A. D. Wieck and A. Devi, Low temperature growth of gallium oxide thin films via plasma enhanced atomic layer deposition, *Dalton Trans.*, 2017, **46**, 16551–16561, DOI: [10.1039/C7DT03427J](https://doi.org/10.1039/C7DT03427J).
  - 25 E. R. Borujeny, O. Sendetskyi, M. D. Fleischauer and K. C. Cadien, Low thermal budget heteroepitaxial gallium oxide thin films enabled by atomic layer deposition, *ACS Appl. Mater. Interfaces*, 2020, **12**, 44225–44237, DOI: [10.1021/acsami.0c08477](https://doi.org/10.1021/acsami.0c08477).
  - 26 Y. Meng, Y. Gao, K. Chen, J. Lu, F. Xian, L. Xu, G. Zheng, W. Kuang and Z. Cao, Annealing induced phase transitions and optical properties of Ga<sub>2</sub>O<sub>3</sub> thin films synthesized by sputtering technique, *Optik*, 2021, **244**, 167515, DOI: [10.1016/j.ijleo.2021.167515](https://doi.org/10.1016/j.ijleo.2021.167515).





- 27 M. Rebien, W. Henrion, M. Hong, J. P. Mannaerts and M. Fleischer, Optical properties of gallium oxide thin films, *Appl. Phys. Lett.*, 2002, **81**, 250–252, DOI: [10.1063/1.1491613](#).
- 28 S. Ghose, M. S. Rahman, J. S. Rojas-Ramirez, M. Caro, R. Droopad, A. Arias and N. Neved, Structural and optical properties of  $\beta$ -Ga<sub>2</sub>O<sub>3</sub> thin films grown by plasma-assisted molecular beam epitaxy, *J. Vac. Sci. Technol., B: Nanotechnol. Microelectron.: Mater., Process., Meas., Phenom.*, 2016, **34**, 02L109, DOI: [10.1116/1.4942045](#).
- 29 W. Li, Y. Peng, C. Wang, X. Zhao, Y. Zhi, H. Yan, L. Li, P. Li, H. Yang, Z. Wu and W. Tang, Structural, optical and photoluminescence properties of Pr-doped  $\beta$ -Ga<sub>2</sub>O<sub>3</sub> thin films, *J. Alloys Compd.*, 2017, **697**, 388–391, DOI: [10.1016/j.jallcom.2016.12.143](#).
- 30 P. Schurig, M. Courturier, M. Becker, A. Polity and P. J. Klar, Optimizing the stoichiometry of Ga<sub>2</sub>O<sub>3</sub> grown by RF-magnetron sputter deposition by correlating optical properties and growth parameters, *Phys. Status Solidi A*, 2019, **216**, 1900385, DOI: [10.1002/pssa.201900385](#).
- 31 J. Lee, L. Gautam, F. H. Teherani, E. V. Sandana, P. Bove, D. J. Rogers and M. Razeghi, Investigation of enhanced heteroepitaxy and electrical properties in  $\kappa$ -Ga<sub>2</sub>O<sub>3</sub> due to interfacing with  $\beta$ -Ga<sub>2</sub>O<sub>3</sub> template layers, *Phys. Status Solidi A*, 2023, 2200559, DOI: [10.1002/pssa.202200559](#).
- 32 Y. Oshima, E. G. Villora and K. Shimamura, Halide vapor phase epitaxy of twin-free  $\alpha$ -Ga<sub>2</sub>O<sub>3</sub> on sapphire (0001) substrates, *Appl. Phys. Express*, 2015, **8**, 055501, DOI: [10.7567/APEX.8.055501](#).
- 33 A. Barthel, J. Roberts, M. Napari, M. Frentrop, T. Huq, A. Kovács, R. Oliver, P. Chalker, T. Sajavaara and F. Massabuau, Ti alloyed  $\alpha$ -Ga<sub>2</sub>O<sub>3</sub>: route towards wide band gap engineering, *Micromachines*, 2020, **11**, 1128, DOI: [10.3390/mi11121128](#).
- 34 Y. Xu, C. Zhang, Y. Cheng, Z. Li, Y. Cheng, Q. Feng, D. Chen, J. Zhang and Y. Hao, Influence of carrier gases on the quality of epitaxial corundum-structured  $\alpha$ -Ga<sub>2</sub>O<sub>3</sub> films grown by mist chemical vapor deposition method, *Materials*, 2019, **12**, 3670, DOI: [10.3390/ma12223670](#).
- 35 Y. Zuo, Q. Feng, T. Zhang, X. Tian, W. Li, J. Li, C. Zhang, J. Zhang and Y. Hao, A novel method for growing  $\alpha$ -Ga<sub>2</sub>O<sub>3</sub> films using mist-CVD face-to-face heating plates, *Nanomaterials*, 2023, **13**, 72, DOI: [10.3390/nano13010072](#).
- 36 M. Hilfiker, R. Korlacki, R. Jinno, Y. Cho, H. G. Xing, D. Jena, U. Kilic, M. Stokey and M. Schubert, Anisotropic dielectric functions, band-to-band transitions, and critical points in  $\alpha$ -Ga<sub>2</sub>O<sub>3</sub>, *Appl. Phys. Lett.*, 2021, **118**, 062103, DOI: [10.1063/5.0031424](#).
- 37 A. Segura, L. Artús, R. Cuscó, R. Goldhahn and M. Feneberg, Band gap of corundumlike  $\alpha$ -Ga<sub>2</sub>O<sub>3</sub> determined by absorption and ellipsometry, *Phys. Rev. Mater.*, 2017, **1**, 024604, DOI: [10.1103/PhysRevMaterials.1.024604](#).
- 38 M. Kracht, A. Karg, M. Feneberg, J. Bläsing, J. Schörmann, R. Goldhahn and M. Eickhoff, Anisotropic optical properties of metastable (01–12)  $\alpha$ -Ga<sub>2</sub>O<sub>3</sub> grown by plasma-assisted molecular beam epitaxy, *Phys. Rev. Appl.*, 2018, **10**, 024047, DOI: [10.1103/PhysRevApplied.10.024047](#).
- 39 M. Feneberg, J. Nixdorf, M. D. Neumann, N. Esser, L. Artús, R. Cuscó, T. Yamaguchi and R. Goldhahn, Ordinary dielectric function of corundumlike  $\alpha$ -Ga<sub>2</sub>O<sub>3</sub> from 40 meV to 20 eV, *Phys. Rev. Mater.*, 2018, **2**, 044601, DOI: [10.1103/PhysRevMaterials.2.044601](#).
- 40 H. Y. Playford, A. C. Hannon, E. R. Barney and R. I. Walton, Structures of uncharacterized polymorphs of gallium oxide from total neutron diffraction, *Chem. – Eur. J.*, 2013, **19**, 2803–2813, DOI: [10.1002/chem.201203359](#).
- 41 I. Cora, F. Mezzadri, F. Boschi, M. Bosi, M. Čaplovičová, G. Calestani, I. Dódoný, B. Pécz and R. Fornari, The real structure of  $\epsilon$ -Ga<sub>2</sub>O<sub>3</sub> and its relation to  $\kappa$ -phase, *CrystEngComm*, 2017, **19**, 1509–1516, DOI: [10.1039/c7ce00123a](#).
- 42 J. Kim, D. Tahara, Y. Miura and B. G. Kim, First-principle calculations of electronic structures and polar properties of ( $\kappa$ , $\epsilon$ )-Ga<sub>2</sub>O<sub>3</sub>, *Appl. Phys. Express*, 2018, **11**, 061101, DOI: [10.7567/APEX.11.061101](#).
- 43 E. Dobročka, F. Gucmann, K. Hušková, P. Nádaždy, F. Hrubíšák, F. Egyenes, A. Rosová, M. Mikolášek and M. Ľapajna, Structure and thermal stability of  $\epsilon/\kappa$ -Ga<sub>2</sub>O<sub>3</sub> films deposited by liquid-injection MOCVD, *Materials*, 2023, **16**, 20, DOI: [10.3390/ma16010020](#).
- 44 L. Aarik, H. Mändar, J. Kozlova, A. Tarre and J. Aarik, Atomic layer deposition of Ga<sub>2</sub>O<sub>3</sub> from GaI<sub>3</sub> and O<sub>3</sub>: Growth of high-density phases, *Cryst. Growth Des.*, 2023, **23**, 5899–5911, DOI: [10.1021/acs.cgd.3c00502](#).
- 45 X. Cao, Y. Xing, J. Han, J. Li, T. He, X. Zhang, J. Zhao and B. Zhang, Crystalline properties of film grown on c-sapphire by MOCVD and solar-blind ultraviolet photodetector, *Mater. Sci. Semicond. Process.*, 2021, **123**, 105532, DOI: [10.1016/j.msssp.2020.105532](#).
- 46 Y. Oshima, E. G. Villora, Y. Matsushita, S. Yamamoto and K. Shimamura, Epitaxial growth of phase-pure  $\epsilon$ -Ga<sub>2</sub>O<sub>3</sub> by halide vapor phase epitaxy, *J. Appl. Phys.*, 2015, **118**, 085301, DOI: [10.1063/1.4929417](#).
- 47 Y. Li, X. Xiu, W. Xu, L. Zhang, H. Zhao, Z. Xie, T. Tao, P. Chen, B. Liu, R. Zhang and Y. Zheng, Pure-phase  $\kappa$ -Ga<sub>2</sub>O<sub>3</sub> layers grown on c-plane sapphire by halide vapor phase epitaxy, *Superlattices Microstruct.*, 2021, **152**, 106845, DOI: [10.1016/j.spmi.2021.106845](#).
- 48 U. U. Muazzami, P. S. Chavan, R. Muralidharan, S. Raghavan and D. N. Nath, Optical properties of mist CVD grown  $\kappa$ -Ga<sub>2</sub>O<sub>3</sub>, *Semicond. Sci. Technol.*, 2022, **37**, 055011, DOI: [10.1088/1361-6641/ac6129](#).
- 49 J. Aarik, A. Aidla, A. Jaek, M. Leskelä and L. Niinistö, In situ study of a strontium  $\beta$ -diketonate precursor for thin film growth by atomic layer epitaxy, *J. Mater. Chem.*, 1994, **4**, 1239–1244, DOI: [10.1039/JM9940401239](#).
- 50 L. Aarik, H. Mändar, P. Ritslaid, A. Tarre, J. Kozlova and J. Aarik, Low-temperature atomic layer deposition of  $\alpha$ -Al<sub>2</sub>O<sub>3</sub> thin films, *Cryst. Growth Des.*, 2021, **21**, 4220–4229, DOI: [10.1021/acs.cgd.1c00471](#).
- 51 R. Swanepoel, Determination of the thickness and optical constants of amorphous silicon, *J. Phys. E: Sci. Instrum.*, 1983, **16**, 1214–1222, DOI: [10.1088/0022-3735/16/12/023](#).



- 52 W. Q. Hong, Extraction of extinction coefficient of weak absorbing thin films from special absorption, *J. Phys. D: Appl. Phys.*, 1989, **22**, 1384–1385, DOI: [10.1088/0022-3727/22/9/024](https://doi.org/10.1088/0022-3727/22/9/024).
- 53 Y. Oshima, K. Kawara, T. Oshima and T. Shinohe, In-plane orientation control of (001)  $\kappa$ -Ga<sub>2</sub>O<sub>3</sub> by epitaxial lateral overgrowth through a geometrical natural selection mechanism, *Jpn. J. Appl. Phys.*, 2020, **59**, 115501, DOI: [10.35848/1347-4065/abbc57](https://doi.org/10.35848/1347-4065/abbc57).
- 54 V. I. Nikolaev, A. Y. Polyakov, A. V. Myasoedov, I. S. Pavlov, A. V. Morozov, A. I. Pechnikov, I.-H. Lee, E. B. Yakimov, A. A. Vasilev, M. P. Scheglov, A. I. Kochkova and S. J. Pearton, Editors' Choice—Structural, Electrical, and Luminescent Properties of Orthorhombic  $\kappa$ -Ga<sub>2</sub>O<sub>3</sub> Grown by Epitaxial Lateral Overgrowth, *ECS J. Solid State Sci. Technol.*, 2023, **12**, 115001, DOI: [10.1149/2162-8777/ad0888](https://doi.org/10.1149/2162-8777/ad0888).
- 55 H. Siimon and J. Aarik, Thickness profiles of thin films caused by secondary reactions in flow-type atomic layer deposition reactors, *J. Phys. D: Appl. Phys.*, 1997, **30**, 1725–1728, DOI: [10.1088/0022-3727/30/12/006](https://doi.org/10.1088/0022-3727/30/12/006).
- 56 M. Kirm, J. Aarik, M. Jürgens and I. Sildos, Thin Films of HfO<sub>2</sub> and ZrO<sub>2</sub> as potential scintillators, *Nucl. Instrum. Methods Phys. Res., Sect. A*, 2005, **537**, 251–255, DOI: [10.1016/j.nima.2004.08.020](https://doi.org/10.1016/j.nima.2004.08.020).
- 57 J. Aarik, H. Mändar, M. Kirm and L. Pung, Optical characterization of HfO<sub>2</sub> thin films grown by atomic layer deposition, *Thin Solid Films*, 2004, **466**, 41–47, DOI: [10.1016/j.tsf.2004.01.110](https://doi.org/10.1016/j.tsf.2004.01.110).
- 58 J. Furthmüller and F. Bechstedt, Quasiparticle bands and spectra of Ga<sub>2</sub>O<sub>3</sub> polymorphs, *Phys. Rev. B*, 2016, **93**, 115204, DOI: [10.1103/PhysRevB.93.115204](https://doi.org/10.1103/PhysRevB.93.115204).
- 59 T. Kobayashi, T. Gake, Y. Kumagai, F. Oba and Y. Matsushita, Energetics and electronic structure of native point defects in  $\alpha$ -Ga<sub>2</sub>O<sub>3</sub>, *Appl. Phys. Express*, 2019, **12**, 091001, DOI: [10.7567/1882-0786/ab3763](https://doi.org/10.7567/1882-0786/ab3763).
- 60 T. Kawamura and T. Akiyama, Bandgap engineering of  $\alpha$ -Ga<sub>2</sub>O<sub>3</sub> by hydrostatic, uniaxial, and equibiaxial strain, *Jpn. J. Appl. Phys.*, 2022, **61**, 021005, DOI: [10.35848/1347-4065/ac468f](https://doi.org/10.35848/1347-4065/ac468f).
- 61 U. U. Muazzam, R. Muralidharan, S. Raghavan and D. N. Nath, Investigation of optical functions, sub-bandgap transitions, and Urbach tail in the absorption spectra of Ga<sub>2</sub>O<sub>3</sub> thin films deposited using mist-CVD, *Opt. Mater.*, 2023, **145**, 114373, DOI: [10.1016/j.optmat.2023.114373](https://doi.org/10.1016/j.optmat.2023.114373).
- 62 T. Ma, X. Chen, F. Ren, S. Zhu, S. Gu, R. Zhang, Y. Zheng and J. Ye, Heteroepitaxial growth of thick  $\alpha$ -Ga<sub>2</sub>O<sub>3</sub> film on sapphire (0001) by MIST-CVD technique, *J. Semicond.*, 2019, **40**, 012804, DOI: [10.1088/1674-4926/40/1/012804](https://doi.org/10.1088/1674-4926/40/1/012804).
- 63 T. Oshima, T. Nakazono, A. Mukai and A. Ohtomo, Epitaxial growth of  $\gamma$ -Ga<sub>2</sub>O<sub>3</sub> films by mist chemical vapor deposition, *J. Cryst. Growth*, 2012, **359**, 60–63, DOI: [10.1016/j.jcrysgro.2012.08.025](https://doi.org/10.1016/j.jcrysgro.2012.08.025).
- 64 D. Mergel, Modeling thin TiO<sub>2</sub> films of various densities as an effective optical medium, *Thin Solid Films*, 2001, **197**, 216–222, DOI: [10.1016/S0040-6090\(01\)01403-1](https://doi.org/10.1016/S0040-6090(01)01403-1).
- 65 L. Aarik, H. Alles, A. Aidla, T. Kahro, K. Kukli, J. Niinistö, H. Mändar, A. Tamm, R. Rammula, V. Sammelselg and J. Aarik, Influence of process parameters on atomic layer deposition of ZrO<sub>2</sub> thin films from CpZr(NMe<sub>2</sub>)<sub>3</sub> and H<sub>2</sub>O, *Thin Solid Films*, 2014, **565**, 37–44, DOI: [10.1016/j.tsf.2014.06.052](https://doi.org/10.1016/j.tsf.2014.06.052).
- 66 K. Möls, L. Aarik, H. Mändar, A. Kasikov, T. Jõgiaas, A. Tarre and J. Aarik, Influence of  $\alpha$ -Al<sub>2</sub>O<sub>3</sub> template and process parameters on atomic layer deposition and properties of thin films containing high-density TiO<sub>2</sub> phases, *Coatings*, 2021, **11**, 1280, DOI: [10.3390/coatings11111280](https://doi.org/10.3390/coatings11111280).
- 67 S. Ohta, T. Sekiya and S. Kurita, Pressure dependence of optical properties of anatase TiO<sub>2</sub> single crystal, *Phys. Status Solidi B*, 2001, **223**, 265–269, DOI: [10.1002/1521-3951\(200101\)223:1<265::AID-PSSB265>3.0.CO;2-R](https://doi.org/10.1002/1521-3951(200101)223:1<265::AID-PSSB265>3.0.CO;2-R).
- 68 B. G. Kim, Epitaxial strain effect on the band gap of a Ga<sub>2</sub>O<sub>3</sub> wide bandgap material, *J. Korean Phys. Soc.*, 2021, **79**, 946–952, DOI: [10.1007/s40042-021-00304-x](https://doi.org/10.1007/s40042-021-00304-x).
- 69 Y.-B. Wang, P. Han, Q. Chen and M. Willander, Scattered refractive index profiles of thin silicon oxide film on silicon substrate, *J. Appl. Phys.*, 1997, **82**, 5868–5870, DOI: [10.1063/1.366404](https://doi.org/10.1063/1.366404).
- 70 A. Kasikov, A. Tarre and M. Marandi, Dispersion of chromia films (eskolaite) in UV-VIS, *J. Electr. Eng.*, 2019, **70**, 36–43, DOI: [10.2478/jee-2019-0039](https://doi.org/10.2478/jee-2019-0039).

